



National Library
of Canada

Bibliothèque nationale
du Canada

Acquisitions and
Bibliographic Services Branch

Direction des acquisitions et
des services bibliographiques

395 Wellington Street
Ottawa, Ontario
K1A 0N4

395, rue Wellington
Ottawa (Ontario)
K1A 0N4

Your file *Voire référence*

Our file *Notre référence*

NOTICE

AVIS

The quality of this microform is heavily dependent upon the quality of the original thesis submitted for microfilming. Every effort has been made to ensure the highest quality of reproduction possible.

La qualité de cette microforme dépend grandement de la qualité de la thèse soumise au microfilmage. Nous avons tout fait pour assurer une qualité supérieure de reproduction.

If pages are missing, contact the university which granted the degree.

S'il manque des pages, veuillez communiquer avec l'université qui a conféré le grade.

Some pages may have indistinct print especially if the original pages were typed with a poor typewriter ribbon or if the university sent us an inferior photocopy.

La qualité d'impression de certaines pages peut laisser à désirer, surtout si les pages originales ont été dactylographiées à l'aide d'un ruban usé ou si l'université nous a fait parvenir une photocopie de qualité inférieure.

Reproduction in full or in part of this microform is governed by the Canadian Copyright Act, R.S.C. 1970, c. C-30, and subsequent amendments.

La reproduction, même partielle, de cette microforme est soumise à la Loi canadienne sur le droit d'auteur, SRC 1970, c. C-30, et ses amendements subséquents.

UNIVERSITY OF ALBERTA

Volumetric Impedance Model of Gastric Contractile Activity

BY



Wing-Chau Kee

A thesis submitted to the Faculty of Graduate Studies and Research in partial fulfillment of the requirements for the degree of Master of Science.

DEPARTMENT OF ELECTRICAL ENGINEERING

Edmonton, Alberta

Fall, 1992



National Library
of Canada

Bibliothèque nationale
du Canada

Canadian Theses Service Service des thèses canadiennes

Ottawa, Canada
K1A 0N4

The author has granted an irrevocable non-exclusive licence allowing the National Library of Canada to reproduce, loan, distribute or sell copies of his/her thesis by any means and in any form or format, making this thesis available to interested persons.

The author retains ownership of the copyright in his/her thesis. Neither the thesis nor substantial extracts from it may be printed or otherwise reproduced without his/her permission.

L'auteur a accordé une licence irrévocable et non exclusive permettant à la Bibliothèque nationale du Canada de reproduire, prêter, distribuer ou vendre des copies de sa thèse de quelque manière et sous quelque forme que ce soit pour mettre des exemplaires de cette thèse à la disposition des personnes intéressées.

L'auteur conserve la propriété du droit d'auteur qui protège sa thèse. Ni la thèse ni des extraits substantiels de celle-ci ne doivent être imprimés ou autrement reproduits sans son autorisation.

ISBN 0-315-77146-1

Canada

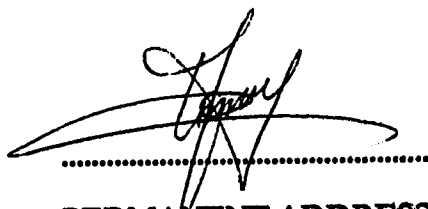
UNIVERSITY OF ALBERTA

RELEASE FORM

NAME OF AUTHOR: Wing-Chau Kee
TITLE OF THESIS: Volumetric Impedance Model of
Gastric Contractile Activity
DEGREE: Master of Science
YEAR THIS DEGREE GRANTED: 1992

Permission is hereby granted to the University of Alberta Library to reproduce single copies of this thesis and to lend or sell such copies for private, scholarly or scientific purposes only.

The author reserves all other publication and other rights in association with the copyright in the thesis, and except as hereinbefore provided neither the thesis nor any substantial portion thereof may be printed or otherwise reproduced in any material form whatever without the author's prior written permission.



PERMANENT ADDRESS:


2909 Block Q
Kornhill, Quarrybay,
Hong Kong

Date: August 27, 1992

UNIVERSITY OF ALBERTA


FACULTY OF GRADUATE STUDIES AND RESEARCH

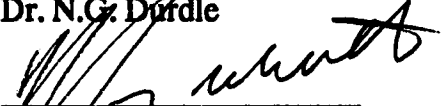
The undersigned certify that they have read, and recommend to the Faculty of Graduate Studies and Research for acceptance, a thesis entitled **Volumetric Impedance Model of Gastric Contractile Activity** submitted by Wing-Chau Kee in partial fulfillment of the requirements for the degree of Master of Science.


Dr. Z.J. Koles (co-supervisor)


Dr. K. L. Bowes (co-supervisor)


Dr. Y.J. Kingma


Dr. N.G. Durdle


Dr. R. Rajotte (external Examiner)

Date: August 19, 1992

ABSTRACT

Many gastric diseases, such as gastric ulcer, gastritis and postvagotomy syndrome, may be associated with an abnormality in gastric contractile activity (GCA) and the gastric electrical activity (GEA). In order to monitor this activity, both invasive and non-invasive methods are available. One of the approaches is the method of impedance epigastrography(IE). This technique is non-invasive and it measures the gastric contractile activity indirectly. IE requires an impedance monitoring device that records the change in gastric impedance cutaneously. Electrodes are applied in a tetrapolar electrode configuration in which an alternating current(4mA, 100kHz) is applied to the body through two of the electrodes. The other two electrodes measure the change in electric potential which in turn reflects the change in the shape of the stomach. Hence, gastric contractile activity can be monitored cutaneously.

The measurement accuracy of IE depends largely on the placement of these four electrodes. Unfortunately, there are no proven best locations where the electrodes should be placed. In this study, a three-dimensional model consisting of 4466 resistors was used to simulate the human torso. The optimal electrode locations were found with the model. The resistors were arranged in layers and vertically inter-connected. The model was simulated with SPICE (Simulation Program with Integrated Circuit Emphasis) to determine the node voltages. Then, three TURBO C++ programs were used to determine

the optimal electrode placements and to display the voltage profile of the torso surface.

After the optimal electrode locations were found, actual IEs were measured from three volunteers to validate the SPICE model. The SPICE electrode placement was found to record better epigastric impedance signals than the standard electrode placement. Also, the IE recorded with the new placement scheme demonstrated high correlation with the electrogastrogram.

ACKNOWLEDGEMENTS

I wish to express my deepest gratitude to Professor Y. J. Kingma, Dr. Z. J. Koles and Dr. K. L. Bowes for their invaluable assistance and guidance, and to Dave Rudyk for his help.

Also, I would like to thank all the volunteers for their help and commitment.

Contents

List of Tables	x
List of Figures	xi
List of Abbreviations	xiii
I Introduction	1
II The Stomach	4
2.1 Gastric Physiology	4
2.2 Gastric Motility	5
2.3 Gastric Emptying	7
2.4 Electrogastric Activity	8
III The Measurement of Gastric Motility	13
3.1 Invasive Methods	13
3.1.1 Radiology	13
3.1.2 Electromyography	14
3.1.3 Scintigraphy	15
3.2 Non-invasive Methods	16
3.2.1 Gastric-Ultrasonography	16
3.2.2 Electrogastrography	17
3.2.3 Impedance Methods	18
IV Applied Potential Tomography and Impedance Epigastrography	19
4.1 Brief History	19
4.2 Principles of The Impedance Methods	20
4.3 Tissue, Current Pathways and Equipotential Lines	24
4.4 Applied Potential Tomography for Monitoring Gastric Emptying	26
4.5 Impedance Epigastrography for Monitoring Gastric Emptying	27

V	Three Dimensional Modelling of the Stomach with SPICE	38
5.1	The Effects of Current Magnitude and Frequency on Tissue and Electrode Behavior	38
5.2	The Electrode Placement Problem	39
5.3	Modelling the Torso and Stomach	40
5.4	Resistor Model for Impedance Epigastrography	42
5.5	SPICE Resistor Modelling of the Stomach	43
5.6	Analysis of the Stomach Models	45
5.6.1	Center Stomach Model	46
5.6.2	Results and Discussion	46
5.6.3	Frontal Stomach Model	48
5.6.4	Results and Discussion	48
5.7	Analysis of the Complete Torso Model	49
5.7.1	Antral Contraction	51
5.7.2	Results and Discussion	51
5.7.3	Corpus Contraction	52
5.7.4	Results and Discussion	52
5.8	Conclusions	53
VI	Experimental Validation of the 3-D SPICE Model	75
6.1	Introduction	75
6.2	SPICE Electrode Placement vs Standard Electrode Placement	76
6.2.1	Procedures	76
6.2.2	Results and Discussion	77
6.3	IE Signal Validation with the EGG	78
6.3.1	Procedures	78
6.3.2	Results and Discussion	78
6.3.2.1	Before Ingestion	79
6.3.2.2	After Ingestion	79
6.4	Conclusions	80
6.5	Suggestion for Future Research	81
	Bibliography	105

List of Tables

4.1	Resistivity values for mammalian tissue	30
5.1	Resistivity values for mammalian tissue used in Kim <i>et al.</i> 's(1988) 3-D Finite Element Model for Impedance cardiography	55
5.2	Reference for layer and node numbering	56
5.3	ΔV_{MAX} of various current and voltage electrode locations for center stomach model analysis	58
5.4	ΔV_{MAX} of various current and voltage electrode locations for frontal stomach analysis	59
5.5	ΔV_{MAX} of various current and voltage electrode locations for complete torso model: antral contraction analysis	60
5.6	ΔV_{MAX} of various current and voltage electrode locations for complete torso model: corpus contraction analysis	61

List of Figures

2.1	Physiological anatomy of the stomach. The two main regions of the stomach: body and antrum.	11
2.2	Membrane potential in the smooth muscle. The period of the slow wave is approximately 20 seconds. Contractions occur when there is ERA	12
4.1	Volume conductor with tetra-polar electrode configuration	31
4.2	Current paths in cell structures at high and low frequencies	32
4.3	Equipotential lines on a conducting cell when current I is being applied with two plate electrodes	33
4.4	Equipotential lines in a conducting cell distorted by the introduction of a conductor and an insulator	34
4.5	Point current source applied on both sides or one side of the conducting cell	35
4.6	Standard electrode placement for measuring epigastric impedance	36
4.7	A typical trace from a fasting individual of gastric emptying as measured by impedance epigastrography	37
5.1	Typical layer of the SPICE resistor phantom	62
5.2	Schematic drawings of the three stomach models	63
5.3	Three-dimensional representation of resistor cubes	64
5.4	Cross section of the resistor phantom for center stomach model and frontal stomach model analyses.	65
5.5	Stomach model used in center stomach model and frontal stomach model analyses	66
5.6	Optimal electrode locations in center stomach model	67
5.7	Optimal electrode locations in frontal stomach model	68
5.8	A typical cross-section of the resistor phantom at the level of the antrum for the complete torso model	69
5.9	Stomach model used in the complete torso model analysis (a) antral (b) corpus contraction analysis	70
5.10	Optimal electrode locations for the complete torso model: antral contraction analysis	71
5.11	Optimal electrode locations for the complete torso model: corpus contraction analysis	72
5.12	Voltage profile for the complete torso model: antral contraction analysis	73
5.13	Voltage profile for the complete torso model: corpus contraction analysis	74

6.1	Schematic diagram of the Impedance Monitoring Device	83
6.2	IE recordings of the SPICE scheme and the standard scheme before and after ingestion of food (Volunteer A)	84
6.3	Recordings of IE after digital bandpass filtering (0.02Hz-0.1Hz)	85
6.4a	Recordings of IE before ingestion (Volunteer B)	86
6.4b	Recordings of IE after ingestion (Volunteer B)	87
6.5a	Recordings of IE before ingestion, after bandpass filtering	88
6.5b	Recordings of IE after ingestion, after bandpass filtering	89
6.6	Frequency spectrum of the IE from experiment A(VolunteerA)	90
6.7	Frequency spectrum of the IE from experiment A(VolunteerB)	91
6.8a	Power spectral arrays of recordings from Volunteer A	92
6.8b	Power spectral arrays of recordings from Volunteer B	93
6.9	Location of EGG electrodes and the IE electrodes in Experiment B	94
6.10a,b,c	IE and EGG of Experiment B, before ingestion (Volunteer C)	95 - 97
6.11	Time-Frequency Plot of IE and EGG before and after ingestion	98
6.12	Cross spectral array between IE and EGG (before ingestion)	99
6.13a,b,c	IE and EGG of Experiment B, after ingestion (Volunteer C)	100 - 102
6.14	Power spectral arrays of IE and EGG after ingestion (Volunteer C)	103
6.15	Cross spectral arrays between IE and EGG after ingestion (Volunteer C)	104

List of Abbreviations

3-D	three-dimensional
A-A	anterior-anterior
A-P	anterior-posterior
A-S	anterior-side
AC	alternating current
Ag/AgCl	silver / silver chloride
APT	applied potential tomography
CAD	computer aided design
cpm	cycle per minute
DTPA	di-ethylene-triamine-penta-acetic acid
ΔV_{MAX}	maximum potential difference across two voltage electrodes in the SPICE analysis
ECA	electrical control activity
ECG	electrocardiogram
EGG	electrogastrogram
EIT	electrical impedance tomography
ERA	electrical response activity
FFT	Fast Fourier Transform
FSN	Full Spectrum Normalization
GCA	gastric contractile activity
GEA	gastric electric activity
IE	impedance epigastrography
MMC	migrating motility complex
p-p	peak to peak
PE2	Personal Editor II
PQR	characteristic wave form of the ECG
PSA	power spectral array
S-S	side-side
SNR	signal to noise ratio
SPICE	simulation program with integrated circuit emphasis
SSN	Separate Spectrum Normalization
VDU	visual display unit

To My Parents

I. INTRODUCTION

In 1921 Walter Alvarez reported that electrodes placed on the abdomen permitted recording of gastric electrical potential (Alvarez *et al.*, 1922). Alvarez's experiment was repeated later in 1975 by Brown *et al.* (1975). Brown's discovery aroused the general interest in the development of new methods for the diagnosis of gastro-intestinal diseases. The EGG has become the focus of many researchers.

The diagnostic ability of the EGG remains in doubt. The PQR complex and T wave which appear on the ECG have made it a powerful, useful and reliable technique for the diagnosis of cardiac disease. As the stomach wall contains a large amount of smooth muscle tissue which depolarizes periodically, it is believed that there should also be diagnostic value to the EGG. Unfortunately, the electric-potential signal of the stomach muscle is much weaker than that of the heart. Also, the signal to noise ratio (SNR) of the recorded signals does not permit much further development of the EGG for clinical use. The desire for such a non-invasive technique has however led to another method, the Impedance Epigastrogram (IE). This method resembles the applied potential tomogram (APT), sometimes referred to as electrical impedance tomogram (EIT). In IE, an alternating current is applied to the torso surface via two current electrodes and two similar electrodes are used to measure the potential differences at various locations on the torso. However, APT requires intensive mathematical computations for generation of a two dimensional image. A computational algorithm for the generation of a three dimensional

image is not yet available. The back projection technique used in conventional computed tomography does not apply to APT. This is because the paths which the currents travel are hard to predict. For IE, the inverse problem is not a concern because its purpose is only to detect the internal impedance changes due to the change in the shape of the stomach.

For IE, only four electrodes are required. And, because of this, the SNR, sensitivity, accuracy and the reproducibility of this method depends largely on the proper locations of these four electrodes. Models have been used to study the paths along which the current travels. The resistor phantom is an example but it is technically difficult to built a three dimensional resistor model. With the help of circuit simulation programs and faster computer processors, a large resistor phantom is possible. In this study, a simulated resistor phantom is constructed containing more than 4000 resistors, arranged in a ten-layer interconnected lattice. Each layer has 299 resistors and the shape of the stomach can be reasonably incorporated. This model is used to estimate optimal locations for the four electrodes.

Since IE detects the change of shape of the stomach, it reflects gastric motility. It may become a useful method for the diagnosis of gastric diseases. There are three main types of abnormal motility patterns related to gastric diseases: fast rhythm (tachygastric), slow rhythm (bradygastric) and irregular rhythm (arrhythmia) (Camilleri and Malagelada, 1984)(Kim, 1988). If any of these rythms is accompanied by contractions, it might be observable using IE. IE is

non-invasive and the measuring equipment is relatively inexpensive and simple to use.

II. THE STOMACH

2.1 GASTRIC PHYSIOLOGY

The stomach is an important organ in the digestive system. Without its grinding and mixing ingested food with gastric juices, the intestine alone could not perform its absorption function. The stomach can be divided into two major regions, the proximal stomach and the distal stomach. The cardia is the region representing the transition between the esophagus and the stomach (Dobois, 1983). Anatomically, the stomach also can be divided into two major parts: the body and the antrum, as shown on FIG.2.1.

The stomach relaxes during feeding and it allows a cavity for the accommodation of a large volume of incoming food. Food materials are pushed towards the antrum by peristaltic waves which originate in the body. The waves travel along the antrum to the pylorus. The antrum is composed of a thick wall of muscle. It coordinates with the body during the propulsion of gastric contents towards the pylorus. The pylorus is the distal opening of the stomach. The circular muscle layer is 50 to 100 per cent greater than in the earlier portions of the antrum; the circular muscle is sometimes called the pyloric sphincter. The pylorus maintains same tone most of the time but is often slightly open. The opening is large enough for water and other fluids to pass easily. The pylorus controls the passage of larger materials through the gastric outlet to the duodenum (Schulze, *et al.*,1984). Also, it prevents reflux of duodenal material which contains basic bile substances and

pancreatic enzymes from entering the stomach and damaging the gastric mucosa.

The stomach itself has a smooth muscle wall. There are two main layers of muscle: the outer longitudinal muscle layer and the inner circular muscle layer. The serosa lies on the outer surface of the longitudinal muscle layer whereas the submucosa and the mucosa lie on the inner surface of the circular muscle layer. The circular muscle layer thickens in the antral region and crests a thick band of muscle at the most distal part of the stomach constituting the pylorus. This circular muscle is not continuous to the duodenum but rather separated by a septum which forms a groove and marks the transition between duodenal and the gastric mucosa (Sheiner, 1979).

2.2 GASTRIC MOTILITY

Motility patterns of the stomach are very complex. There are three motor functions contributed from the contractile activities of the smooth muscle of the stomach. First, when a meal is initially ingested, the stomach relaxes to accommodate the swallowed material. The storing process results in a large intragastric volume increase with only slight increase in intragastric pressure (less than 10mmHg/2L). Secondly, gastric contractions cause mixing of ingested materials with gastric secretions to form a semifluid mixture called chyme. Thirdly, during digestion of a meal, the contractions of pylorus and antrum discharge gastric materials into the small intestine at a rate suitable for proper digestion and absorption by the small intestine. At the final

stage of digestion, the remaining gastric contents are swept out of the stomach by forceful and periodic contractions of the antrum into the duodenum (Schulze *et al.*, 1984).

There are three main types of contractile activities. The first type is, as mentioned above, receptive relaxation and accommodation. During swallowing, the oral region of the stomach relaxes for the accommodation of the incoming material. The intragastric volume increases and the increase is accompanied with very little increase in intragastric pressure (less than 10mmHg/2L). The second type is tonic contraction. Tonic contraction occurs in the oral region during the digestion of a meal. The result is the pushing of intragastric contents towards the caudal regions and a little mixing of the material with the gastric juice. The third type is peristaltic contractile activity. It consists of rhythmic contraction which begins in the body of the stomach. This peristaltic constrictor wave moves toward the antrum along the stomach wall. The wave of contraction increases both in strength and speed as it approaches the duodenum. The period of each complete sweep of contraction wave is approximately 20 seconds. Some of the waves become so intense that they provide powerful peristaltic constrictor rings. The contractile motion provides movement of the intragastric contents and causes mixing and grinding of the material. The result of the sweeping is: (1)small food particles are expelled out into the duodenum through the pylorus; (2)most of the antral contents are squirted backward toward the body of the stomach. (Guyton, 1992).

During interdigestive periods, the activity of several organs of the gastrointestinal tract exhibits a specific integrated pattern (Schulze

et al., 1984; Weisbrodt, 1984). For the stomach, the pattern consists of several phases of activity which happen cyclically. After emptying of most of the final materials in the stomach by strong peristaltic contractions, the stomach rests for a long period of time. During the interdigestive periods, there are intermittent phases of 3-10 minutes intense contractions, which are known as the actuating front of the migrating motility complex, the MMC (Dobois, 1983; Grundy and Scratcherd, 1984; Schulze *et al.*, 1984).

2.3 GASTRIC EMPTYING

The process of gastric emptying has attracted most of the attention. It has been suggested that up to 75% of patients with functional gastrointestinal symptoms have abnormalities in gut motility (Malagelada and Stanghellini, 1985). Peristaltic contractions are the major driving force of the emptying process. Most of the time the peristaltic contractions are weak. They cause the mixing of food with the gastric secretions. Nevertheless, about one fifth of the time the antral contractions become very intense. The contractions spread through the antrum as strong peristaltic, ringlike constrictions. The continuous peristaltic contractions push more contents towards the duodenum but only a very small amount of content can enter the duodenum through the pyloric opening. Gastric contents with diameter less than 2mm are expelled into the duodenum (Dobois, 1983). Larger gastric contents are squirted backward to the body of the stomach. They are pushed towards the antrum again by the tonic contraction of

the stomach where they are trapped by the next peristaltic wave (Dobois, 1983; Ehrlein and Akkermans, 1984). The amount of emptying depends on several factors, force of peristaltic contraction, tone of the oral region of the stomach, the contractile activity of the pylorus and the contractile activity of the duodenum (Sheiner, 1979). Approaching the end of the emptying period, the contractions begin farther and farther up the body of the stomach. These contractions tend to propel any remaining undigested contents in the duodenum. Then, the stomach returns to the originally relatively empty state, the fasting state (Dobois, 1983).

2.4 ELECTROGASTRIC ACTIVITY

Contractions of the gastrointestinal tract are mainly under the control of phasic depolarizations of the smooth muscle membrane potentials. There are two types of myoelectrical activity which are responsible for the muscle contractions of the stomach, the electrical control activity (ECA) and the electrical response activity (ERA), as shown in FIG.2.2. The ECA is vacuously known as slow waves, the basic electrical rhythm or the control potential. ECA controls the frequency of the rhythmic contractions. The ECA is a pacemaker type of signal which has a frequency about three cycles per minute (3cpm) or 0.05Hz. It is generated by the spontaneous depolarizations and successive repolarizations of the smooth muscle cell membrane (Kim, 1988). These cyclically recurring electrical potentials mainly originate from the smooth muscle cells of the distal two-thirds of the stomach

(Smout and Van der Schee, 1989). Also, it was found that there is a definite gradient of intrinsic frequencies of the ECA; the frequencies are higher near the corpus region at the greater curvature and gradually decreasing towards the pylorus. The ECA spreads quickly and circumferentially and then propagates slowly through the antrum as a ring of excitation determining when contraction can occur (Grundy and Scratcherd, 1984; Kingma, 1989; Smout and Van der Schee, 1989). When the tissue of the smooth muscle is intact, the oscillating regions are electrically coupled and the lower frequencies are pulled up to the highest intrinsic frequency. Because the regions more distal to the pacemaker region have a lower intrinsic frequency, they tend to lag behind the pacemaker signal when being pulled up to the intrinsic frequency. The frequency gradient in a circular direction is much less than in the longitudinal direction. The net result is that the depolarization wave will appear as a ring of activity travelling towards the antrum (Grundy and Scratcherd, 1984; Kingma, 1989).

The intrinsic wave is always present (Smout and Van der Schee, 1989), but it does not usually cause contraction of the stomach muscle. Contraction occurs only when there is ERA, the spike potential. The spike potentials appears automatically when the resting membrane potential of the smooth muscle becomes less negative than -40mV level. The normal membrane resting potential is about -55mV and it varies. Also, the higher the membrane potential rises above the -40mV level, the larger the frequency of the spike potential. The strength of muscle contraction is related to the frequency of the spike potential. Since the ERA occurs on top of the ECA, when contractions occurs, the

contraction wave travels with the ECA towards the distal direction. FIG.2.2 shows the relationship among the ECA, the ERA and the smooth muscle contractile activity (Dobois, 1983; Kingma, 1989; Sarna, 1989).

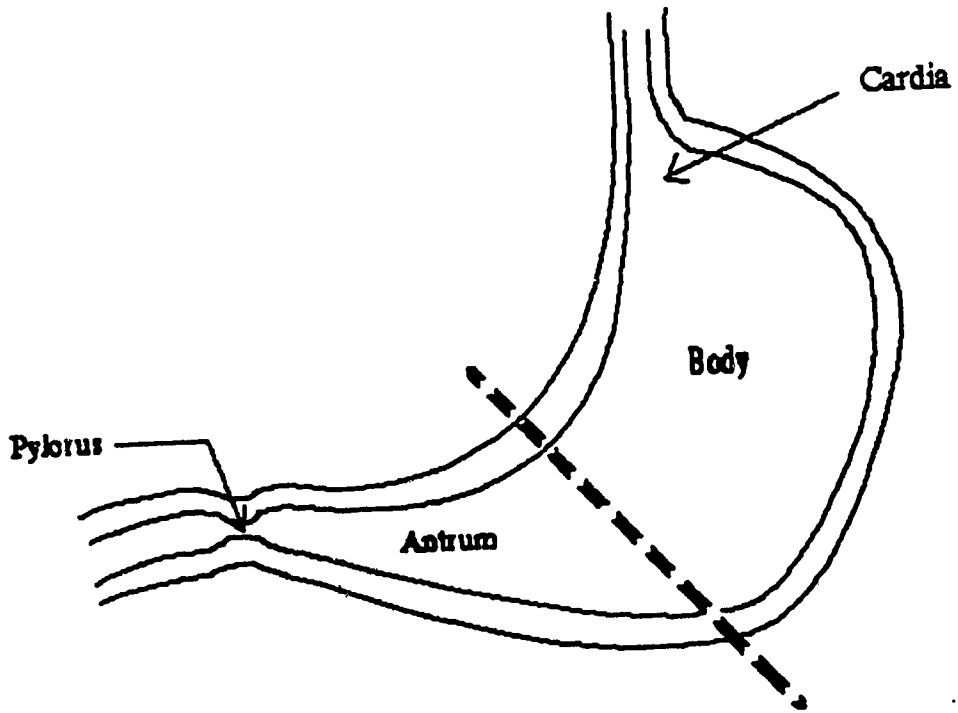


Figure 2.1 Physiological anatomy of the stomach.
The two main regions of the stomach:
body and antrum.

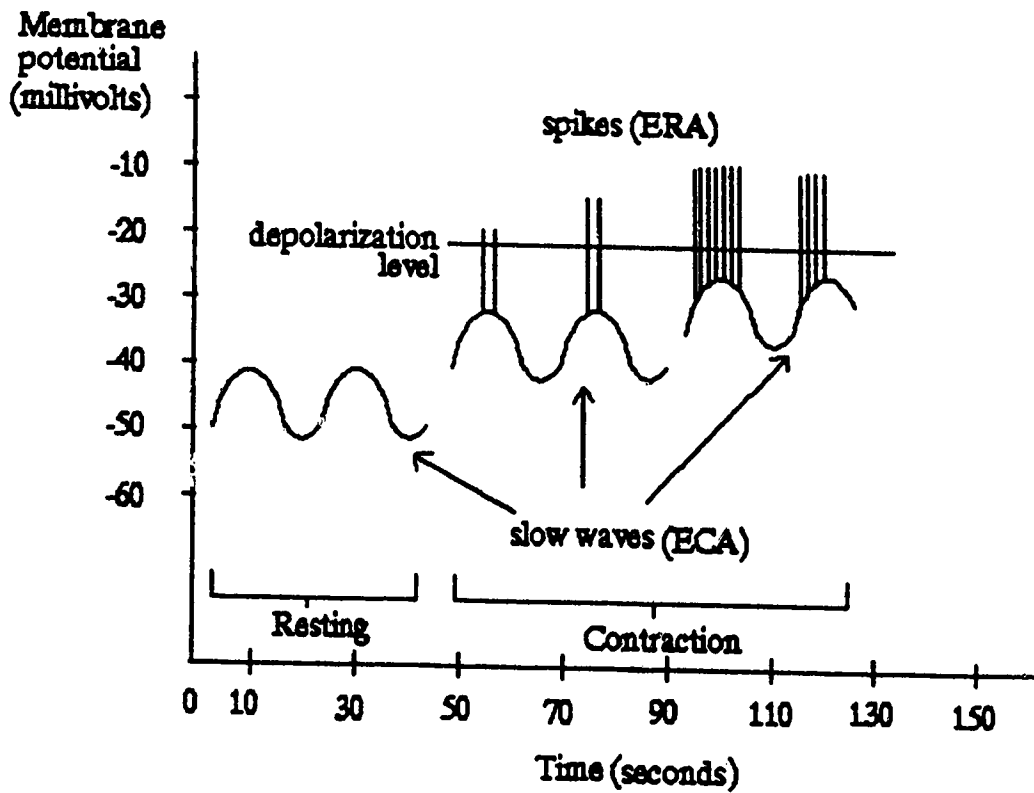


Figure 2.2 Membrane potential in the smooth muscle. The period of the slow wave is approximately 20 seconds. Contractions occur when there is ERA. (adapted from Guyton, 1992)

III. THE MEASUREMENT OF GASTRIC MOTILITY

Some abdominal disorders are probably caused by an increased or decreased rate of gastric emptying (Dobois, 1983). For example, gastric retention can be related to peptic ulcer disease, diabetes, collagen disease, and etc; enhanced gastric emptying can be related to dumping symptoms, postgastrectomy disorder, peptic ulcer disease and etc. Therefore, by observing the motility of the stomach, certain gastric diseases can be diagnosed. Several methods have been developed to observe the motility of the stomach. They can be categorized into two main divisions: invasive and non-invasive.

3.1 INVASIVE METHODS

3.1.1 RADIOLOGY

Radiology provides qualitative or semiquantitative information on the motor behavior of the alimentary canal (Corazziari and Torsoli, 1988). The application of radiology to the stomach is usually done by mixing a meal with some materials which can show good contrast on X-ray images, for example mixing beef with barium (Dobois, 1983). X-ray images can indirectly show the stomach wall contractions, and hence reveal the motor activity of the stomach. However, the use of radiology is limited because of the harmful ionizing radiation. Only a limited

number of studies can be performed (Corazziari and Torsoli, 1988; Heading, 1984; Read, 1989) and a few short-lasting motor events can be detected. Therefore, it cannot provide quantification of the collected data (Corazziari and Torsoli, 1988).

3.1.2 ELECTROMYOGRAPHY

Electromyography of the stomach is the extracellular recording of electrical potential changes originating from smooth muscle of the stomach wall. Alvarez and Machoney in 1922 reported the first myoelectrical activity recorded on the serosal surface of the stomach (Alvarez and Machoney, 1922). The recorded signals originate in the smooth muscle of the stomach and can be correlated with events occurring in the smooth muscle cells in the region of interest. In electromyography, extracellular electrodes are used on the smooth muscle. The recordings illustrate the integration of the changes in membrane potential from both the ECA and the ERA. From the phase, frequency and amplitude of these signals, diagnosis is possible. Also, a triphasic gastric potential can be shown (Soper and Sarr, 1988). Electromyography provides a reliable and excellent recording of gastric electrical activity with minimal background noise. The recordings represent the synchronized activity of thousands of gastric smooth muscle cells which are in direct contact with the electrodes (Stoddard, 1984). Various electrodes are used for the measurement. Serosal electrodes are mounted on the serosal layer of the stomach and the arrangement is implemented during operation. However, general

clinical use is limited. Intraluminal electrodes are mounted on a probe with a gastroscope or using the nasal entry and put into the stomach. Adhesion to the mucosa is made by suction electrodes. Prolonged use of such electrodes causes bleeding of the mucosa (Kingma, 1989). Also, the recordings are very sensitive to mechanical artifacts. Although electromyography has been performed successfully in the stomach, interpretation of the recordings for diagnostic purpose is still in its infancy. Also, the invasive nature and its relative practicality to other techniques are the major drawbacks of this technique.

3.1.3 SCINTIGRAPHY

Scintigraphy is a simple, inexpensive and nontoxic method technique for the observation of gastric emptying. It avoids the need for sampling of intragastric contents and is highly acceptable to patients (Horowitz and Akkermans, 1989). In this method, a radiopharmaceutical agent, such as ^{99m}Tc -DTPA, is incorporated into a liquid, solid, or mixed solid and liquid meal and is taken orally (Gustavsson, 1988). In this analysis, a gamma camera is used for the detection of radionuclide tracers. Also, a computer-assisted gamma camera with a large field of view is used as a standard equipment for motility studies (Gustavsson, 1988). However, results of the method contain a geometrical error as most radionuclide methods evaluate a three-dimensional process in a two-dimensional manner (Horowitz and Akkermans, 1989). For the analysis of gastric emptying, the relationship between gastric emptying and the detected radionuclide

amount is not uniform due to various factors: gamma ray attenuation, Compton scatter and septal penetration (Horowitz and Akkermans, 1989). Moreover, superimposition of the stomach and small intestine makes it difficult to distinguish between an emptied or retained meal (Gustavsson, 1988). Although this method is considered as the most accurate and clinically applicable method for the detection of disordered gastric emptying, a potential problem arises from the close contact of the radioactive test meal with the mucosa and the radiation exposure has to be taken into consideration. Especially, the gonads of the female will be at risk as the radioactive materials will be staying in the colon during the analysis. Hence, the exposure of radiation has limited the frequency of use of this technique.

3.2 NON-INVASIVE METHODS

3.2.1 GASTRIC-ULTRASONOGRAPHY

Ultrasonic scanning of the stomach was first attempted for the detection and examination of gastric disease in 1973 (Lutz, 1973). The technique has moved towards ultrasound imaging. With real time imaging, reliable techniques for studying the motility of the gastroduodenal region are being developed (Hau *et al.*, 1989). The ultrasound image of the ultrasonography is a two dimensional representation of the intraluminal space. It provides a dynamic display of the movement of various organs within the body. For the technique

to be feasible in the echo-free fluid filled lumen of the stomach, a test meal containing certain sized particles is used and detected by the ultrasound technique (King and Heading, 1988). Peristaltic activity and gastric emptying can be recorded directly on videotape. This method permits area and linear measurements for the gastric activities. The playback of the video allows assessments of the results and selection of optimal images for study after the scanning (Mamtora and Thompson, 1989). The method is non-invasive, repeatable and radiation-free. However, the equipment is relatively expensive and not all patients are capable of taking the special meal before ultrasonography.

3.2.2 ELECTROGASTROGRAPHY

Electrical activity of the stomach can also be monitored by measuring electrogastric activity with cutaneous electrodes. This method was first demonstrated by Walter Alvarez in 1921 with a string galvanometer (Alvarez, 1922). This method is non-invasive and avoids the possible risk of exposure to radiation. Hence, it is safe to adults and infants. The electrogastrogram (EGG) technique resembles the method of the electrocardiogram (ECG); it measures the electrical activity of the stomach wall smooth muscles on the abdominal surface. Essentially, the EGG extracellular electrodes record the cyclically recurring electrical activity, the ECA, of the smooth muscle cells of the distal two thirds of the stomach but no ECA from the fundus (Smout and Van der Schee, 1989).

The EGG signal is not sufficient to reflect the contractile activity of the stomach (Smout and Van der Schee, 1989). With implanted force transducers, serosal and cutaneous electrodes in conscious dogs, Smout *et al.*(1980) were able to show that, EGG signals reflected both ECA and ERA (Schee and Smout, 1989). In general, but not always, ECA is observable on the EGG during gastric motor quiescence and the EGG signal increases with the intensity of ERA. Although the non-invasive nature of EGG makes itself a good alternative to invasive electromyography, there are many technical problems. The EGG recording is not as promising as that of the ECG. The diagnostic capability of the EGG is still at its infancy. EGG is still not a clinically relevant technique for diagnostic purposes (Smout and Van der Schee, 1989; Smout *et al.*, 1980).

3.2.3 IMPEDANCE METHODS

Impedance methods for studying gastric emptying are considered to be the least invasive. These methods are non-toxic and without radiation. There are a few limitations for diagnosis of gastric diseases (Dawids, 1987). The following section is dedicated to the principles and methodologies of different impedance techniques used to monitor gastric emptying.

IV. THE MONITORING OF GASTRIC EMPTYING

4.1 BRIEF HISTORY

The use of electrical impedance techniques for biological purposes was started as early as 1932. Atzler and Lehmann detected an ultra-high frequency (100MHz) (Atzler *et al.*, 1932) impedance change with bipolar electrodes from cardiac contractile activity. Later in the 1940's, Nyboer was able to measure thoracic impedance changes synchronous with the cardiac cycle with a tetrapolar electrode configuration (Nyboer *et al.*, 1940). Not only cardiac activity and pulmonary activity but also gastric activities can be analyzed with impedance methods. The recorded impedance changes on the surface of the body can be used to construct images of the internal body. Although scintigraphy is so far the most satisfying method for measuring gastric emptying, it is expensive and it requires ingestion of radioactive isotopes. Applied Potential Tomography (APT) and Impedance Epigastrography (IE) are the possible alternatives to scintigraphy. The impedance method is based on the fact that the impedance change of a volume conductor is proportional to the change in potential at the measuring electrodes when the current is kept constant (Kothapalli and Durdle, 1989). Although the spatial resolution of impedance imaging is not as good as that of scintigraphy, the simple, the cheap and non-invasive nature of the impedance method has made it worthwhile to develop. Both APT and IE use the changes in electrical resistivity to follow gastric emptying (Mangnall,

1989). At present, the most promising clinical application of APT is for the assessment of gastric emptying (Dawids, 1987).

4.2 PRINCIPLES OF THE IMPEDANCE METHODS

The basis of IE can be reduced to Ohm's Law.

$$V = I * Z ; \quad 4.2.1$$

where V [Volts] is the potential difference across the body which has an impedance Z [Ω] as a current I [Amps] passes through it. But being more sophisticated, Geselowitz(1971) and Lehr(1972) have considered the following. Four electrodes are applied to a volume conductor in a tetrapolar electrode configuration, as shown on FIG.4.1. Current I_{12} is impressed through the current electrodes E_1 and E_2 . The resulting electric potential is denoted by ϕ whereas the resulting current density is denoted by J_ϕ . Suppose I_{12} is impressed at time t , and the conductivity is given by g_ϕ . At the same time t , at the measuring electrodes E_3 and E_4 , another current I_{34} is being impressed. The resulting electric potential, current density and conductivity associated with I_{34} are denoted by ψ , J_ψ and g_ψ respectively.

Hence:
$$J_\phi = - g_\phi \nabla \phi, \quad 4.2.2$$

and
$$J_\psi = - g_\psi \nabla \psi. \quad 4.2.3$$

But, from the divergence theorem,

$$\int_V \nabla \cdot A \, dv = \oint_S A \cdot ds \quad 4.2.4$$

If \mathbf{A} is substituted for $\psi \mathbf{J}_\phi$,

$$\begin{aligned} \int_V \nabla \cdot (\psi \mathbf{J}_\phi) dV &= \int_V \psi (\nabla \cdot \mathbf{J}_\phi) + \mathbf{J}_\phi \cdot \nabla \psi dV \\ &= \oint_S \psi \mathbf{J}_\phi \cdot d\mathbf{s} \end{aligned} \quad 4.2.5$$

where $\nabla \cdot \mathbf{J}_\phi = 0$, because there is no active current source in the volume. Therefore,

$$\int_V \mathbf{J}_\phi \cdot \nabla \psi dV = \oint_S \psi \mathbf{J}_\phi \cdot d\mathbf{s} \quad 4.2.6$$

and similarly it follows that

$$\int_V \mathbf{J}_\psi \cdot \nabla \phi dV = \oint_S \phi \mathbf{J}_\psi \cdot d\mathbf{s} \quad 4.2.7$$

From the combination and subtraction of eqn 4.2.6 and eqn 4.2.7, and also the substitution from eqn 4.2.2 and eqn 4.2.3,

$$\int_V (g_\psi - g_\phi) \nabla \phi \cdot \nabla \psi dV = \oint_S (\phi \mathbf{J}_\psi - \psi \mathbf{J}_\phi) \cdot d\mathbf{s} \quad 4.2.8$$

Since $g_\phi = g_\psi = g$, so that $g_\psi - g_\phi = 0$; and therefore,

$$\oint_S (\phi \mathbf{J}_\psi - \psi \mathbf{J}_\phi) \cdot d\mathbf{s} = 0 \quad 4.2.9$$

or

$$\oint_S \phi \mathbf{J}_\psi \cdot d\mathbf{s} = \oint_S \psi \mathbf{J}_\phi \cdot d\mathbf{s} \quad 4.2.10$$

Consider at another time t' , at E_1 and E_2 , the conductivity and the potential distribution of the volume conductor resulting from the same impressed current I_{12} are given by g' and ϕ' respectively; Lehr(1972) showed that, similar to eqn 4.2.8,

$$\int_V (g_\phi - g') \nabla \phi' \cdot \nabla \psi \, dV = \int_S (\psi J_\phi' - \phi' J_\psi) \cdot ds \quad 4.2.11$$

Since the current applied at t and t' is the same, if J_ϕ and J_ϕ' are also the same, then

$$\int_S \psi J_\phi' \cdot ds = \int_S \psi J_\phi \cdot ds \quad 4.2.12$$

Therefore eqn 4.2.10 can be written as:

$$\int_S \phi J_\psi \cdot ds - \int_S \psi J_\phi' \cdot ds \quad 4.2.13$$

And hence, eqn 4.2.11 becomes

$$\int_V (g_\psi - g') \nabla \phi' \cdot \nabla \psi \, dV = \int_S (\phi - \phi') J_\psi \cdot ds \quad 4.2.14$$

If $\Delta g = g_\psi - g'$ and $\Delta \phi_{34} = \phi - \phi'$, dividing eqn 4.2.14 by I_{12} and I_{34} , it becomes

$$\begin{aligned} - \int_V \Delta g \frac{\nabla \phi'}{I_{12}} \cdot \frac{\nabla \psi}{I_{34}} \, dV &= \frac{\Delta \phi_{34}}{I_{12}} \\ &= \Delta Z \end{aligned} \quad 4.2.15$$

where ΔZ denotes the change in impedance. Eqn 4.2.15 is also known as the Geselowitz's equation (Geselowitz, 1971). It states that, if the applied current remains constant from the time t to t' , the change in impedance Z within a volume conductor is proportional to the change in potential distribution $\Delta \phi_{34}$ measured at electrodes E_3 and E_4 . The above equation forms the basis for all impedance methods.

For the application of impedance techniques to human subjects, the volume conductor can represent a volume of body tissue. I_{12} , J_ϕ and ϕ are the electrical characteristics of the volume. Therefore, the

change of ϕ within the body can be reflected by the change of impedance, ΔZ , on the surface of the body.

In the estimation of the cardiac stroke volume from impedance recordings, a model which has been commonly used has been derived and discussed by Penney(1986). With some modification of the model, it can be applied to the antrum of the stomach located inside the torso. Consider the resistance of the gastric contents in the antrum and the antrum itself to be given by

$$R_{f+a}(t) = \frac{\rho_{f+a} l}{A_a(t)} \quad 4.2.16$$

where $R_{f+a}(t)$ is the combined resistance of the antral gastric content and the antrum as a function of time; ρ_{f+a} is the combined resistivity of the antral gastric content and the antrum; l is the length of the antrum and $A_a(t)$ is the cross section area of the antrum as a function of time. If we express

$$A_a(t) = \frac{V_a(t)}{l} \quad 4.2.17$$

then,

$$R_{f+a}(t) = \rho_{f+a} \frac{l^2}{V_a(t)} \quad 4.2.18$$

Defining R_t to be the resistance of the torso and assuming it to be constant throughout the measuring time segment t' , and considering the measured mutual resistance $R_m(t)$ to be the parallel combination of R_t and $R_{f+a}(t)$, we have:

$$\frac{1}{R_m} = \frac{1}{R_{f+a}(t)} + \frac{1}{R_t} \quad 4.2.19$$

Solving for $V_a(t)$ from eqn 4.2.18 and eqn 4.2.19, it yields

$$V_a(t) = \frac{\rho_{f+a} l^2}{R_m(t)} + \frac{\rho_{f+a} l^2}{R_t} \quad 4.2.20$$

From eqn 4.2.20, the volume change of the antrum $V_a(t)$ with respect to the change in the mutual resistance R_m can be found from

$$\frac{\partial V_a(t)}{\partial R_m(t)} = -\frac{\rho_{f+a} l^2}{R_m^2} \quad 4.2.21$$

By approximation of the left hand side of eqn 4.2.21 with $\frac{\Delta V_a}{\Delta R_m}$,

$$\Delta V_a = -\frac{\rho_{f+a} l^2 \Delta R_m}{R_m^2(t)} \quad 4.2.22$$

Although eqn 4.2.22 is just a modification of an equation derived for impedance plethysmography applied on the thoracic region, it suggests the possibility of using impedance epigastrography to estimate gastric emptying.

4.3 TISSUE, CURRENT PATHWAYS AND EQUIPOTENTIAL LINES

Tissues have quite diverse resistivities (Barber, 1989). Some of the values are listed on Table 4.1. The values shown differ significantly and hence indicate that construction of images of resistivities is possible and they should show good contrast. In this method, a high

frequency low amplitude AC current(2-5mA 50k-100kHz) is applied onto the body surface with skin electrodes. Different tissues should have different structures and properties. At low frequency, the current will flow mainly in the intracellular environment, which is the intracellular fluid. So the resistivity of a tissue depends largely on the proportion and distribution of the cells and the size of the conducting pathways (Barber, 1989). As the applied current frequency increases, the penetrating ability of the current into the cellular structure increases. A possible reason for this is that at low frequencies, current will not penetrate cell membranes because of the high reactance of the membrane capacitance, but will penetrate at higher frequencies as the reactive component of the impedance is lower. Hence, for the high frequency measurement, it is affected by both the intracellular and extracellular events inside the body, whereas at low frequency operation, the recording only reflects the extracellular events. Therefore, at high frequencies, the applied current is going more or less in a straight line pathway, as shown on FIG.4.2. Although at high frequencies current penetrates in a straighter pathway, the current flow is three dimensional. Therefore, it is important to understand the current flow pathways and the equipotential lines on the body surface before any correlation of the recording to the change in physiological events can be drawn.

FIG.4.3 shows a simple model for understanding equipotential lines and the current pathways two-dimensionally with current being applied by plate electrodes onto a conducting cell (Baker, 1989). The current density distribution in the cell is uniform and the equipotential

lines are parallel to the electrode plates. But when a highly conducting sphere or an insulating sphere is put between the plates, the field lines are distorted as shown on FIG.4.4a and FIG.4.4b. If, instead, small electrodes are used in place of the plate electrodes, the current density distribution and equipotential lines also will be distorted, as shown on FIG.4.5a and FIG.4.5b for different electrode locations. With these models, we can obtain an idea how the current distributes itself if small current electrodes are applied to the human torso.

4.4 APPLIED POTENTIAL TOMOGRAPHY FOR MONITORING GASTRIC EMPTYING

In 1987, Mangnall *et al.*(1987) and Avill *et al.*(1987) used 16 electrodes around the upper abdomen. They used an 1mA (50kHz) current source and an impedance image was developed. The set up for APT requires a data collection module, a Visual Display Unit (VDU), a computer and a printer(Mangnall, 1989). Sixteen electrodes are placed in a circular array around the torso. A 5mA (peak to peak) 50kHz alternating current is applied across one pair of adjacent electrodes. The potential differences between each other thirteen pairs of adjacent electrodes are recorded. The current electrodes are shifted to the adjacent pair after one set of potential measurements is made. Until each pair of adjacent electrode becomes the current driving electrodes, one cycle of recording is completed. Each data set consists of 150 cycles of recordings. Data are then backprojected to form an image of the change in resistivity across the torso. The image is displayed on the

VDU and the data is stored on the disk. The ability of APT to follow gastric emptying is considered good. Cimetidine must be administered before the test to inhibit the secretion of gastric acids which could cause gastric impedance variations (Mangnall, 1987; Barber *et al.*, 1988). APT has been shown to follow gastric emptying of liquids with high correlation and it can also be used to follow gastric emptying of semi-solid meals such as that consisting mashed potato (Mangnall, 1989). There are certain limitations for APT; however, APT is also responsive to gastric acid secretion and bile reflux (Mangnall, 1989; Barber *et al.*, 1988).

4.5 IMPEDANCE EPIGASTROGRAPHY FOR MONITORING GASTRIC EMPTYING

IE was developed earlier than APT and the principles of operation are similar. IE was first used by McClelland and Sutton (1985) to observe changes in impedance of the epigastrium. Four adhesive Ag/AgCl electrodes were used, two anteriorly and two posteriorly, as shown on FIG.4.6. Impedance changes of 0.80Ω to 1.33Ω were detected (McClelland and Sutton, 1985). In more recent IE applications, an AC (4mA peak to peak, 100kHz) was applied through anterior and posterior electrodes. The change in potential was measured by another pair of anterior-posterior electrodes. Although no image was produced, IE recordings showed the change of impedance across the torso directly. A typical trace is shown on FIG.4.7. A

profile of gastric emptying is obtained. Since IE is very responsive to gastric acid secretion, cimetidine is also required as in APT. IE was found to follow gastric emptying of non-conducting liquids and provide information similar to that of scintigraphy. IE could also be applied to conducting meal if gastric acid secretion is prohibited. Results from IE, as compared to APT, are less reproducible (Mangnall, 1989). The electrode positions of IE are more critical than in the case of APT. IE is very sensitive to body movement and is easily influenced by movement of other internal organs such as the small intestine and the gall bladder. Nevertheless, IE has been found to be able to show gastric emptying in patients with diabetic neuropathy (Gilbey and Watkins, 1987) and for the study of drugs on gastric emptying in normal subjects (McClelland and Sutton, 1986).

Of all the methods for gastric emptying that have been considered, APT and IE can provide reasonable and correlatable results, and are the least invasive and expensive. Also with the help of better computer technology and electronic devices, both methods have plenty of room and potential for improvement and development. Therefore, APT and IE could be the direction in which future gastric diagnostic methodologies will develop. In considering APT and IE, APT can provide better and more reproducible results than IE. However, APT is relatively more intricate to apply than IE. The equipment for IE is much simpler than APT and involves fewer electrodes, but it provides similar information. Also, IE appears to provide accurate and simple measurements of emptying as well as detecting gastric contractile activity (Sutton, 1988). Nevertheless, the

reproducibility of IE is very dependent on the electrode locations. If optimal electrode locations can be found, IE could be an alternate choice to APT for the monitoring of gastric emptying. If this method can be validated, it will be the first method capable of measuring both gastric functions simultaneously (Sutton, 1988). The main difficulty to be overcome is the proper location of the electrodes. At present, a standard electrode placement scheme is used which was proposed by McClelland and Sutton(1985), as shown on FIG.4.6.

Tissue	Resistivity ($\Omega.m$)
Cerebrospinal fluid	0.65
Blood	1.5
Liver	3.5
Human arm	2.4 - 6.75
Skeletal muscle	1.25 - 18.00
Cardiac muscle	1.6 - 7.5
Neural tissue	5.8
Grey matter	2.84
White matter	6.82
Lung	7.2 - 23.6
Fat	27.2
Bone	166

**Table 4.1. Resistivity values for mammalian tissue.
(Brown *et al.*,1985)**

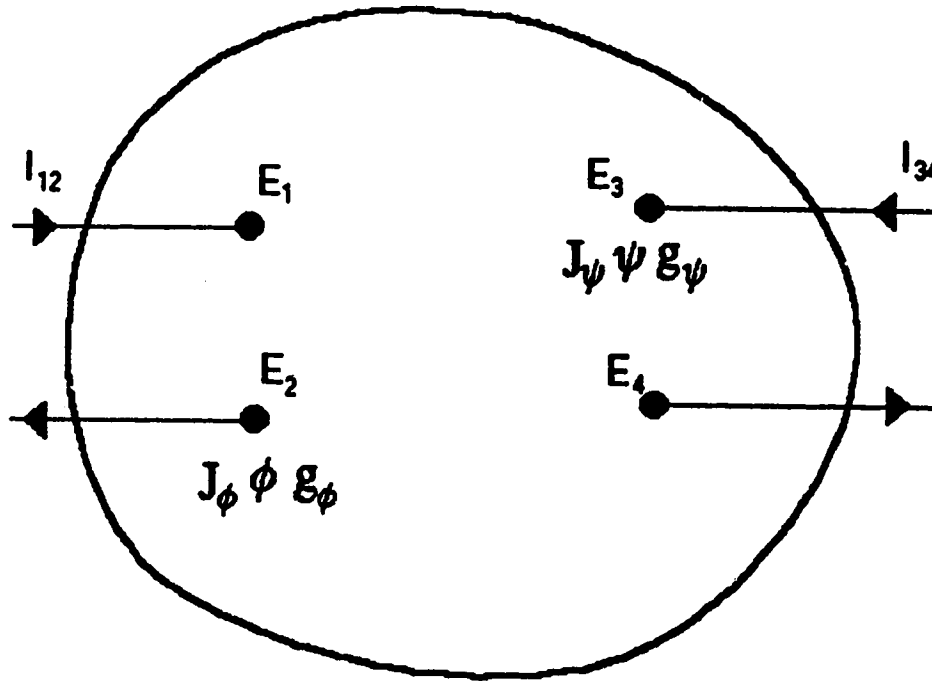


Figure 4.1 Volume conductor with tetra-polar electrode configuration. E_1 and E_2 are current electrodes, where E_3 and E_4 are voltage electrodes. J_ϕ and J_ψ are the current densities; g_ϕ and g_ψ are the conductivities; ϕ and ψ are the electric potentials.

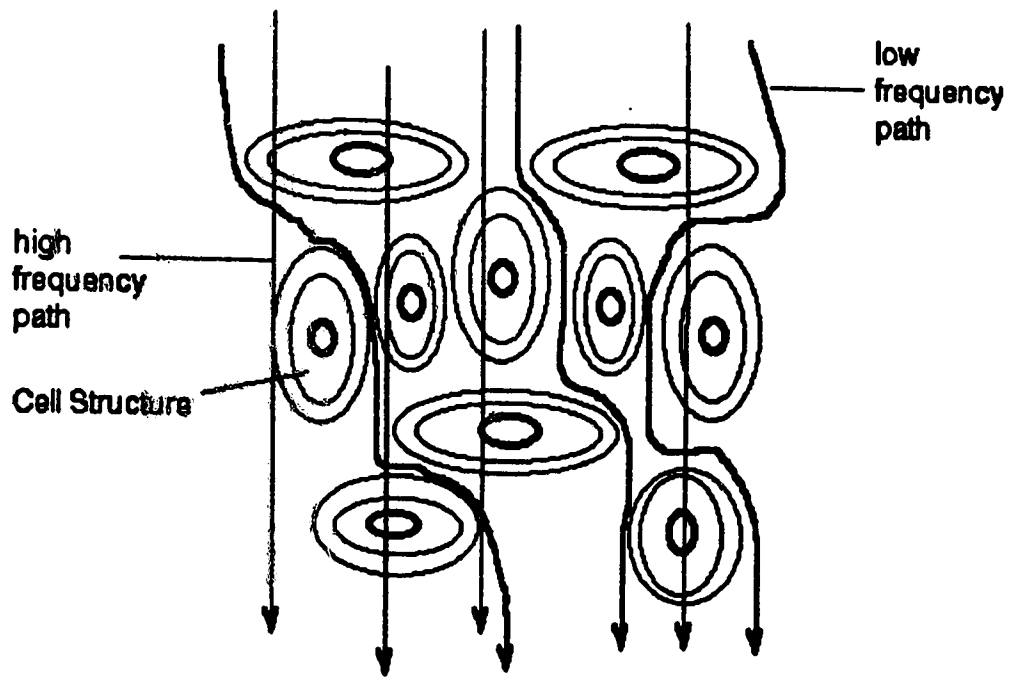


Figure 4.2 At high frequencies, current travels through cell structures in a shorter and more straight path; at lower frequencies, current travels in the extracellular fluid and in a longer path.
(adapted from Barber, 1989)

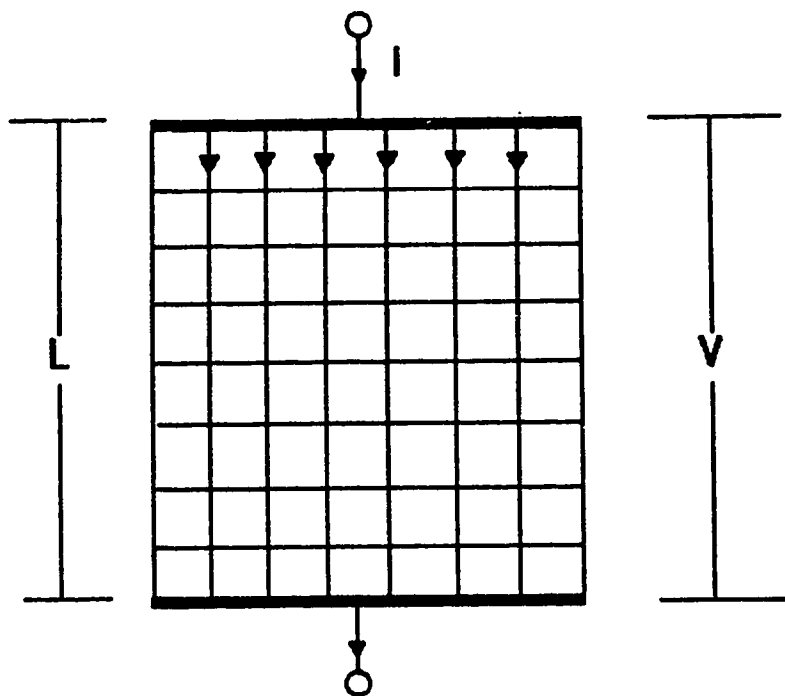


Figure 4.3 Equipotential lines on a conducting cell when current I is being applied with two plate electrodes, where L is the length of the conducting cell and V is the potential across the cell.
(adapted from Baker, 1989)

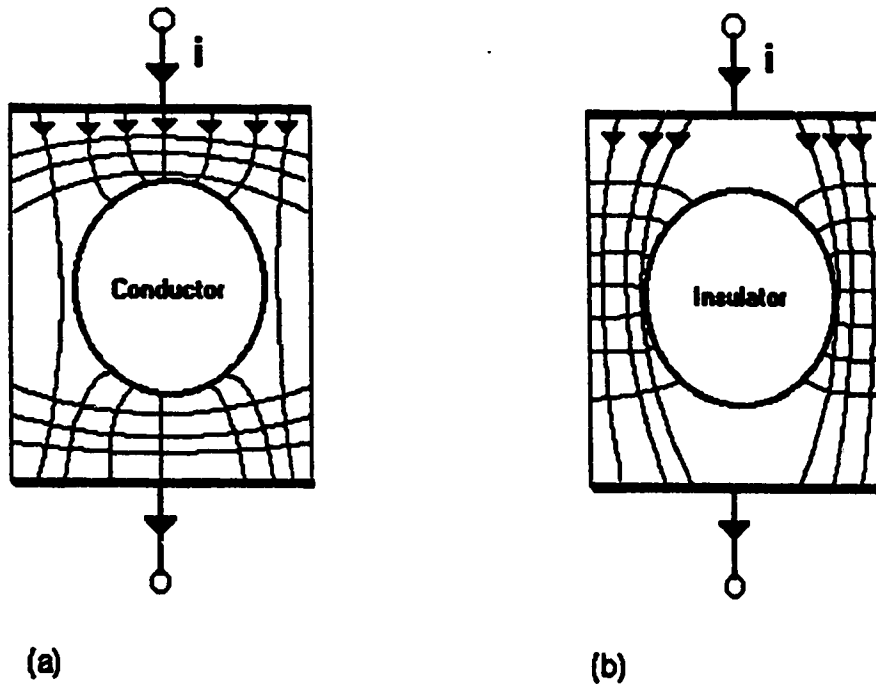


Figure 4.4 (a) Equipotential lines in the conducting cell are distorted by the introduction of a conductor.
 (b) Equipotential lines in the conducting cell are distorted by the introduction of an insulator.
 (adapted from Baker, 1989)

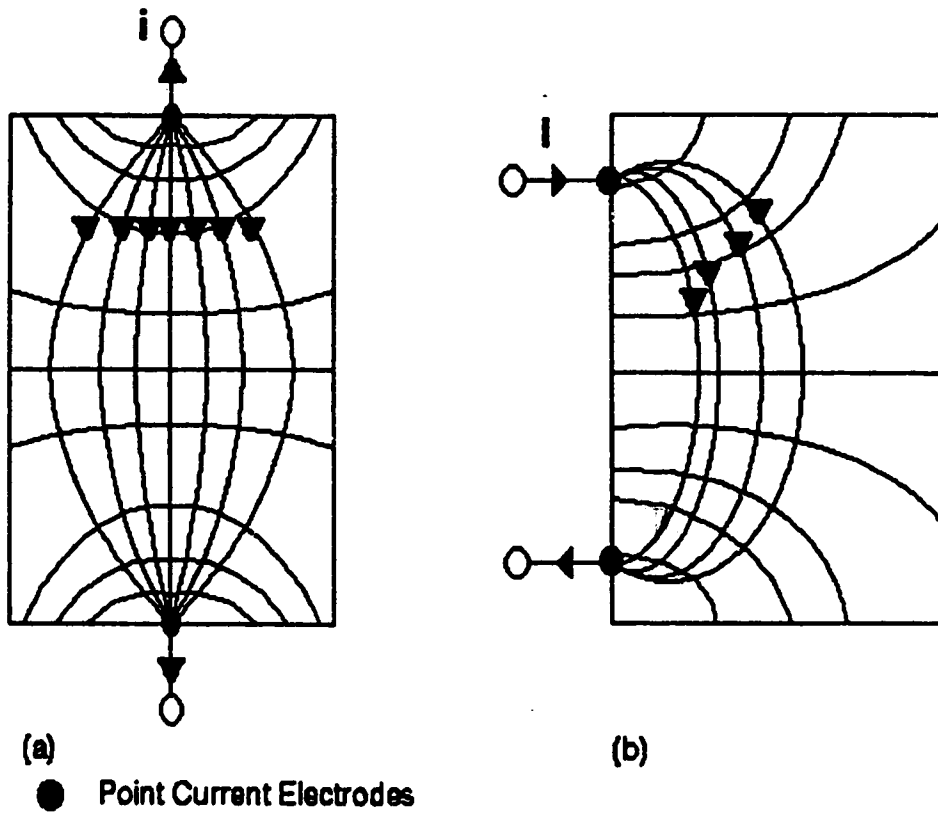


Figure 4.5 (a) Point current source is applied on both sides of the conducting cell.
 (b) Point current source is applied on one side of the conducting cell.
 (adapted from Baker, 1989)

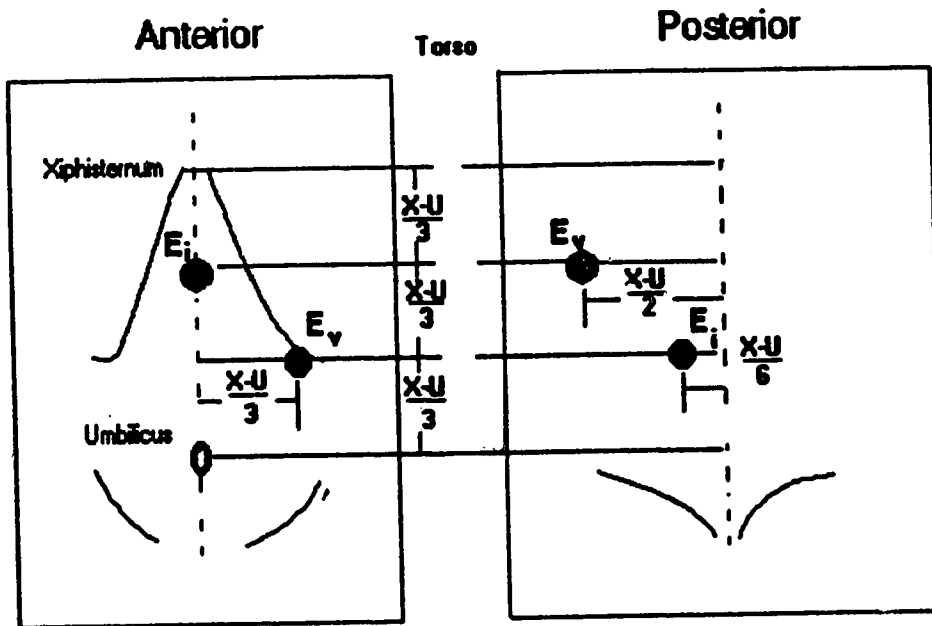


Figure 4.6 Standard electrode placement for measuring epigastric impedance.
 X-U : distance between xiphisternum and umbilicus
 E_i : input current electrodes
 E_v : voltage sensing electrodes
 (adapted from McClelland and Sutton, 1985)

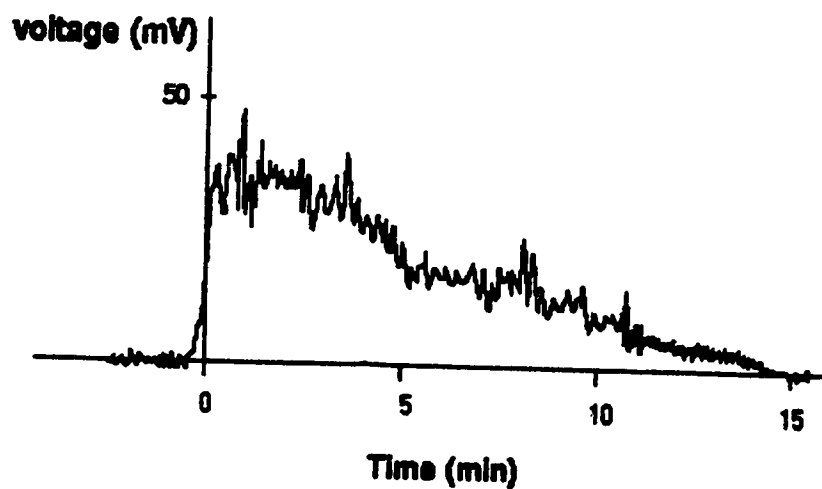


Figure 4.7 A typical trace from a fasting individual of gastric emptying as measured by impedance epigastrography (adapted from Mangnall, 1989)

V. THREE DIMENSIONAL MODELLING OF THE STOMACH WITH S.P.I.C.E.

5.1 THE EFFECTS OF CURRENT MAGNITUDE AND FREQUENCY ON TISSUE AND ELECTRODE BEHAVIOR

Impedance Epigastrography is considered to be an excitation method where a constant AC is applied to the body to detect the changes inside the intraluminal cavity. Constant-current excitation allows the measurement of the impedance information, and the use of AC provides information of both the magnitude and the phase of the impedance changes of the body in the particular AC frequency.

The skin impedance is found to be nonlinear to the applied current magnitude that it drops as the applied current density increases (Qiao and Mørkrid, 1988). Not only the magnitude but also the frequency of the applied current will have effects on the skin impedance. At low frequencies, for 1 cm² of skin, the skin impedance ranges from 10k Ω to 1M Ω whereas at high frequencies it stays around 100 Ω for all electrode locations (Rosell *et al.*, 1988). Therefore, for the IE application, the bulk impedance of the skin and the body is about 250 Ω , which includes the sum of skin and the internal tissue impedance (Newell *et al.*, 1990). However, there is also contact impedance introduced from the skin electrode interface. If only two electrodes are used, the measured voltage would drop as a result of electrode skin contact impedance. To avoid the contact impedance components in the measured voltage, a four electrode scheme has been

used, as shown on FIG.4.6 (Hau *et al.*, 1989; de Vries *et al.*, 1989; Kothapalli and Durdle, 1989).

In IE applications, the Ag/AgCl electrodes are conventionally used because this type of electrode is in thermodynamic equilibrium when used in electrolytes containing Cl-ions (Kingma *et al.*, 1983). The behavior of this type of the electrode can be affected by the frequency of the applied current. The impedance of electrodes increases as the frequency of the applied current decreases (Geddes *et al.*, 1969; Geddes, 1972). Since the IE uses the 100kHz current and the tetrapolar electrode configuration, electrode skin contact impedance should have a minimal influence on the body impedance measurement.

5.2 THE ELECTRODE PLACEMENT PROBLEM

The trend in gastric emptying measurement is toward APT and IE. The APT and IE have about the same capability for diagnosis of gastric activity, and since IE is less complex and expensive, it would seem to be the choice between the two. Electrode placement is a remaining problem for IE. The current pathways and equipotential lines in a homogeneous object from the application of two small current electrodes have been discussed in the previous section. From there, one foresees the difficulty of studying current pathways and equipotential lines when the IE is to be applied to an irregular object, the human torso. Therefore, the placement of electrodes which will provide the best recordings for the IE is not yet known. Nevertheless, IE has been used to monitor the gastric emptying rate with a standard

electrode placement scheme which was proposed and used by McClelland and Sutton(1985), as shown on FIG.4.6 (Sutton, 1988). The electrode locations are identified with reference to the body landmarks, the xiphisternum and the umbilicus. The scheme has been successfully used in the monitoring of gastric emptying. However, for the observation of the gastric contractile activity, this scheme has not been shown to be optimal.

5.3 MODELLING TORSO AND THE STOMACH

Since the location of the electrodes is essentially the critical point for the IE to be a better method to use, one is interested in investigating more thoroughly and in detail the exact and optimal locations for the electrodes. Therefore, models have to be designed to serve the purpose. Many types of modelling are possible: some are highly mathematical and complex, and they do not give a spatial representation of the torso and the stomach. Therefore, it is hard to use these models to investigate the optimal locations for the cutaneous electrodes. An alternative is by finite element modelling. In impedance tomography, many research groups have engaged themselves in developing practical systems for electrical impedance tomography. Different measuring systems and image reconstruction algorithms are studied. Numerical models are also used to simulate APT and to compare different algorithms. Griffiths (1988) developed a two-dimensional physical model to serve the study purposes. The phantom was a square mesh of resistors fastened to a matrix board. Resistors

were chosen to be thermally stable ($0.005\% \text{ } ^\circ\text{C}^{-1}$) and close tolerance (1%). The model was built in such a way that the electrical conductivity of any region of the phantom could be increased by shunting the resistors with additional resistors; also reactance could be introduced by adding capacitors. The phantom was then impressed with a 5mA current and the potential differences were measured by the sixteen electrode configuration around the phantom. The limitation of this type of model is that it only applies to a two-dimensional phantom and it is far more complicated to build a similar three-dimensional model on a circuit board. However, 3-D images can be reconstructed from the 2-D information, Vlachogiannis *et al.*(1988) used a formula developed by Sahalos *et al.*(1986) to approximate the relation between the 2-D and 3-D electrical impedance for impedance measurement of the thorax, which is known as the mean value of the input impedance. However, the equation was specific for thoracic impedance plethysmography. Therefore, a 2 dimensional model is possible of modelling a 3 dimensional torso, but a specific set of formulae has to be defined. Also, whenever the model is modified, a new set of formulae has to be found to approximate the new model. On the other hand, Patterson (1985) has developed a three dimensional model to study the origin of ΔZ due to cardiac activity recorded from band electrodes around the neck and the lower thorax. Volume changes were simulated with resistivity changes in the lungs. 2612 equations were solved using iterative techniques. The three dimensional resistivity model was able to provide information for actual data acquisition, for example the positions for the electrodes and the effects of volume change on the total measured ΔZ . Therefore, a 3-D model is

essential for the determination of the actual spatial electrode locations for impedance epigastrography.

5.4 RESISTOR MODEL FOR IMPEDANCE EPIGASTROGRAPHY

For impedance epigastrography, electrode location is the main problem to be solved. A physical 3-D resistive model is most desirable. The complexity of such a model makes it difficult to use. Even though large resistor phantom can be built, faulty elements are hard to detect. Also, the model is not flexible to any changes such as the change in shape or the location of the stomach. Besides, the optimal locations of the electrodes have to be determined by trial and error. An alternative is to use the SPICE (Simulation Program with Integrated Circuit Emphasis) to simulate a 3-D resistor model. Computer modelling could eliminate all the problems that the physical resistor phantom may have. SPICE is a computer circuit simulation software package. It was first developed and released in 1975 by University of California at Berkeley (Nagel, 1975). SPICE was developed as an alternative to breadboarding for integrated circuit design. SPICE is able to model device behavior which breadboard simulations can not achieve. Also SPICE is available on most mainframes and now also on personal computers.

With SPICE, theoretically any resistor phantom can be modelled, 2-D or 3-D. But for visual convenience and feeling of a physical circuit, *Intusoft* has developed SPICENET with which resistors are connected together in a CAD environment. The limitation of this

SPICE package is that it can only provide a two dimensional connection visually. Therefore, for building a three dimensional model, horizontal layers are built and interconnected by vertical resistors. Each layer consists of homogeneous resistors as shown in FIG.5.1. Resistance of the elements can be adjusted to represent regions of different heterogeneous materials. For the SPICE package developed by *Intusoft*, approximately 1000 interconnected elements can be analyzed with every megabyte of extended memory in the IBM-PC. Connection errors in the net list can also be checked. With this package, manual soldering on breadboard is not required and the risk of having bad connections or faulty elements is avoided.

5.5 SPICE RESISTOR MODELLING OF THE STOMACH

The SPICE is used to build the 3-D phantom of the torso with the stomach inside. The resistor model is composed of ten layers. Each layer has over 300 resistors each of 100Ω . The node numbers are so arranged that the node numbers between adjacent layers differs by 200. This allows the flexibility for the model to be expandable into more layers. Once the net list of the first layer is obtained, all the other layers can be replicated by a text editing program. Also the name of each resistor is given sequentially from left to right as shown in FIG.5.1. The organized structure allows the changes to be made more systematically and easily. There are three resistor models. The first two models contain only the stomach and the homogeneous torso. In the third model, various organs are added to the model. Kim *et al.*

(1988) have used different resistivities for various organs in the three dimensional finite element modelling. With some modifications, the resistivities used in the SPICE model are listed in Table 5.1 and the schematics of the resistor model for the three stages of analyses are as shown on FIG.5.2. The region of the stomach and other organs are assigned different values of resistivity.

The stomach in the first two model spans the second to the seventh layer of the ten-layer model. The first and the last two layers remain homogeneous resistors. For the third model, the stomach spans the first to the seventh layers. All ten horizontal layers of resistors and the vertically interconnected resistors sum to 4626 resistors with 1640 nodes. Table 5.2 shows the relationship between each layer and the node numbers. Since the model contains only resistors, a DC source is used in the place of the AC source. The current is applied to various locations on the edge of the simulated torso. Also 5A is used instead of 5mA so that the impedance (resistance) change can be amplified. From the network analysis with SPICE, a CIRCUIT.OUT file is generated which contains the voltage at all 1640 nodes. The time required for each network analysis is about 68 minutes (with a 80486 microprocessor).

The modelling of the contraction of the antrum and the corpus is obtained by decreasing the size of the antrum or the corpus region of the stomach. Each analysis consists of two SPICE network analysis. One is the model without contraction and the other is the model with contraction. The change in potential difference between two nodes on the torso before and after contraction is found from the analysis. The

change in potential between nodes is an indication of the change in gastric impedance and it is a measure of the contractile activity. The optimal locations of the two current electrodes and two voltage electrodes are found with three Turbo C++ programs: MAXITEN.C, PIX10.C and CHAR10.C. MAXITEN.C reads the two output files, which correspond to before and after contraction of the stomach, from the SPICE and calculates all the changes in potential between every pair of nodes on the surface of the simulated torso. The pair of nodes which has the maximum change in potential difference is marked as the optimal location for the voltage electrodes for the particular application of the current electrodes. PIX10.C and CHAR10.C were developed to produce profiles of the changes in potential difference on the surface of the torso. The images are displayed with color pixels or with text characters respectively. The color image is displayed on the VGA/EGA monitor of the IBM-PC, whereas the text image is ready for printing hard copies. The locations of the four electrodes are indicated.

5.6 ANALYSIS OF THE STOMACH MODELS

The three stomach models are: center stomach model, frontal stomach model and the complete torso model. The stomach is designed in three dimensions with resistor cubes. FIG.5.3 shows a representation of the resistor lattice.

5.6.1 Center Stomach Model

In this model, the stomach is located on the axis A of the torso as shown in FIG.5.4; the antrum is located at the center of the torso and is closer to the anterior of the torso. Contraction of the antrum is modeled by decreasing the number of resistor cubes representing the antrum, from six to three, as shown in FIG.5.5. Current is impressed in various locations on the torso and the change in potential between any two nodes, ΔV 's, are measured. The purpose of this analysis is to identify the possible optimal locations for the electrodes. Table 5.3 is the results of the trials. ΔV_{MAX} is the maximum change in potential difference. Current electrodes are applied in four main orientation: anterior-posterior (A-P), anterior-anterior (A-A), side-side (S-S) and side-anterior (S-A).

5.6.2 Results and Discussion

In the anterior-posterior analysis, current electrodes are located anterior-posteriorly across the antrum. The results of this analysis show that the optimal locations for the voltage electrodes are also anterior-posteriorly oriented, the ΔV_{MAX} is 1.023V. In the anterior-anterior analysis, current electrodes are applied on the anterior surface of the torso only. When the current electrodes are applied vertically, the optimal locations of the voltage electrodes are also vertical on the torso surface. The optimal ΔV_{MAX} is 0.487V. But, this optimal value is less than the half of the optimal value obtained from the anterior-

posterior analysis. In the side-side analysis, the current electrodes are applied on both sides of the torso. The optimal detected voltage change is 0.843V, which is less than the optimal ΔV_{MAX} of the anterior-posterior analysis. In the anterior-side analysis, one current electrode is placed on the anterior side of the torso where the other current electrode is placed on various locations on the sides of the torso. The optimal ΔV_{MAX} is 0.899V and it is still less than that of the anterior-posterior analysis.

From the above analyses, the optimal locations for the current and voltage electrodes are oriented as shown in FIG.5.6; the ΔV_{MAX} is 1.023V. One pair of current and voltage electrodes is on the anterior surface and the other pair is on the posterior surface of the torso. But, since one of the current electrodes is located at the tenth layer, one may suspect that the current is flowing mainly through the ninth and the tenth layer instead of through the torso. An extra layer, the eleventh layer, is added below the tenth layer. The result shows that the ΔV_{MAX} has changed from 1.023V to 0.929V. This is considered minor. And the optimal electrode locations remains the same as the original ten-layer model. Hence, the ten-layer model has been proven to be sufficient for the analysis.

Also, from Table 5.3, the voltage electrodes are located below or at the same level of the current electrodes in most of the cases. This could be the result of the fact that the current pathways are pushed downwards below the corpus level by the corpus resistors. Therefore, the current pathways are mainly below or at the same level of the antrum. Since the change in surface ΔV_{MAX} due to the change in size

of the antrum is caused by the change in current pathways inside the torso, any change in potential difference will be more likely to be detected on the regions below the antrum.

5.6.3 Frontal Stomach Model

After having obtained some understanding of the general locations of the four electrodes, a more realistic case is to be studied. In this model, the stomach is moved more closely to the anterior surface of the torso and closer to the actual location of the human stomach. The contractile activity is expected to be more detectable on the anterior surface. The anterior-posterior, anterior-anterior, side-side and anterior-side analyses are also conducted. Results of this analysis is tabulated in Table 5.4.

5.6.4 Results and Discussion

The results of the anterior-posterior analysis are similar to the results of anterior-posterior analysis of the center stomach model. Optimal locations for the voltage electrodes are also anterior-posteriorly oriented. The optimal ΔV_{MAX} is found to be 4.34V. The voltage electrodes are no longer always located under the current electrodes. In the anterior-anterior analysis, the current electrodes are applied horizontally, vertically and diagonally on the torso surface. The results show that the optimal location of the voltage electrodes is vertical if the current electrodes are vertically applied on the anterior

torso. If the current electrodes are applied diagonally on the anterior surface, the voltage electrodes are found to be diagonally anterior, but the optimal ΔV_{MAX} is larger. The horizontal-anterior orientation of the current electrode is found to be optimal: ΔV_{MAX} is 4.43V. The electrode configuration is as shown in FIG.5.7. The maximum ΔV_{MAX} is also larger than that of the anterior-posterior. The current electrodes overlap the voltage electrodes at (1157,1161). The four electrodes are located directly at the ends of the projection of the antrum on the torso. Also, for a similar set of current electrodes located at (1156,1164) just next to the optimal locations, the result is 2.60V which is just half of the optimal ΔV_{MAX} . Therefore, the optimal locations for electrodes are shown to be extremely sensitive to their orientations. In the side-side and side-anterior analyses, the results are similar to those obtained from the center stomach model analysis. The ΔV_{MAX} s are much less than that of the anterior-posterior and anterior-anterior analyses.

From the above analyses, the optimal current electrode locations are horizontal-anterior-anterior. It is as shown on FIG.5.7.

5.7 ANALYSIS OF THE COMPLETE TORSO MODEL

In the complete torso model analysis, the resistor model is modified to include more simulated organs. The purpose of this analysis is to compare the effect and the relative importance of the

presence of other organs in the intraluminal space to the optimal electrode locations obtained from the previous two stages of analysis. This new model includes the backbone, abdominal muscles, intercostal muscles, liver, spleen, fat tissue and the stomach. A typical cross section of this model is as shown on FIG.5.8. Each region is made up of a different resistivity. Their relative values are listed on Table 5.1. The thoracic muscle is combined with the fat tissues as one layer of tissue. In this model, the skin-electrode contact impedance is ignored since the tetra-polar electrode configuration is used. Also, the impedance of the skin is ignored because it is homogeneous and symmetrical around the body contour. The resistivity of the liver and the spleen is given the same value. The bone component in the model is to model the spine which has the highest resistivity. The stomach itself is surrounded by fat tissue. With this model, two gastric motilities are studied: the contraction of the antrum and the contraction of the corporal region. Hence two sets of optimal electrode locations will be found for different studies. Contraction of the stomach is modelled by changing the resistivities of the antrum or the corpus regions to higher or lower values. MAXITEN.C finds the optimal voltage electrode locations where the change in potential is maximum (ΔV_{MAX}). Anterior-posterior, anterior-anterior, side-side and anterior-side analyses are performed. From the results of the analyses of last two models, the optimal locations for the electrodes occur where the voltage electrodes overlap the current electrodes. Therefore, the initial estimate for the current electrode locations was where the ΔV_{MAX} is found from the previous simulations. The simulation

sequence continues until the optimal voltage electrode locations are the same as the applied current electrode locations.

5.7.1 Antral Contraction

In this analysis, the antral region is represented by the marked region on the 3-D stomach, as shown on FIG.5.9. The contraction of the antrum is modelled by changing the resistance of the region to a lower a resistive value. Again four analyses are performed in the simulation. Results of this analysis are as shown on Table 5.5.

5.7.2 Results and Discussion

In the anterior-posterior analysis, the current electrodes are placed as in the previous two model analysis. If the current electrodes are placed as it has been suggested by McClelland and Sutton (1985), the obtained ΔV_{MAX} is 12.17V. There is no optimal location found since as the iterations went on, the anterior-posterior analysis shifts to anterior-anterior analysis. The results of the anterior-anterior analysis suggest that the optimal electrode locations is (402,1806); the optimal ΔV_{MAX} is 19.74V. The results of the anterior-side analysis are better than the two previous analyses, the optimal ΔV_{MAX} is 25.00V. Finally, the result of the side-side analysis gives the best results of all the analyses. The optimal ΔV_{MAX} is 26.02V which is close to the results of the anterior-side analysis. The optimal location for the tetra-polar

electrode configuration is found in this analysis, which is shown in FIG.5.10.

If the SPICE resistor phantom has modelled the torso correctly, the optimal location for the four electrode configuration would not be as suggested and used by McClelland and Sutton(1985) for the monitoring of gastric emptying. The optimal electrode locations for antral contraction analysis suggested by this analysis is as shown in FIG.5.10. The result predicts that this configuration will be at least twice as effective as the standard four electrode configuration.

5.7.3 Corpus Contraction

In this analysis, the antral region resistivity is kept constant. The corpus region is reduced in size to obtain the optimal locations of the electrodes just for the analysis of corpus contraction. FIG.5.9 shows a 3-D representation of the stomach; the marked region represents the contracting area of the corpus. Again four analyses are performed in the simulation. Results of this analysis are as shown on Table 5.6.

5.7.4 Results and Discussion

From the anterior-posterior analysis, the optimal ΔV_{MAX} is found to be 2.465V. The anterior-anterior analysis provides a optimal ΔV_{MAX} of 3.305V. FIG.5.11 shows the optimal location of the electrodes. The optimal ΔV_{MAX} found from the anterior-side analysis is 2.945V, which

is comparable to the ΔV_{MAX} of the anterior-anterior analysis. Finally from the side-side analysis, the optimal ΔV_{MAX} found is less than of all other three analyses. However, the results are comparable to those of the anterior-posterior analysis. From all the simulations, the results show that the optimal location for the four electrode configuration is found from the anterior-anterior analysis.

5.8 CONCLUSIONS

From the results of the complete torso model analysis, it is suggested that gastric motility could be measured by varying the locations of the electrodes. For corpus contractile activities analysis, current electrodes should be high anterior-anteriorly across the corpus region; whereas for the antral contractile activities analysis, current electrodes should be placed side-side at the antral level. FIG.5.12 and FIG.5.13 are the optimal voltage profiles obtained in the two analyses. The ΔV_{MAX} (3.305V) of the corpus contraction analysis is much smaller than the ΔV_{MAX} (26.02V) of the antral contraction analysis. In fact, if the ΔV is measured with the optimal electrode configuration in the corpus contraction analysis while only the antrum contracts, the ΔV is 11.03V. It is much larger than 3.305V. If the ΔV is measured with the optimal electrode configuration in the antrum contraction analysis while only the corpus contracts, the ΔV is 1.773V which is much smaller than 26.02V. Therefore, it is not possible to monitor the corpus contractile activity with the proposed scheme because it is not be certain whether the measured ΔV is due to the corpus contraction

alone. Also, if the contractile activity from both the antrum and the corpus are present, the resulting signals will be dominated by the antral contractions. Therefore, the new scheme can be used to record antral contractions only. As a conclusion, the optimal electrode placement scheme is as shown on FIG.5.10.

The new electrode placement scheme may not be reliable in practice since it is very vulnerable to motion originating from the intestines and from respiration. The following chapter is dedicated to the validation of the three-dimensional SPICE model. Only the optimal electrode placement scheme proposed for the antral contractions will be studied. Also, the SPICE optimal electrode placement and the standard electrode placement will be compared.

Tissue	Resistivity ($\Omega.m$)
Liver + Spleen	5.00
Fat	15.0
Bone	100.0
Thoracic wall + Muscle + Fat	10.00
Intestine	8.00
Stomach	8.00

Table 5.1 Resistivity values for mammalian tissue used in the SPICE 3-D Finite Element Model for Impedance Epigastrography.

LAYER	NODE NUMBER	
	from	to
1	0	164
2	200	364
3	400	564
4	600	764
5	800	964
6	1000	1164
7	1200	1364
8	1400	1564
9	1600	1764
10	1800	1964

Table 5.2 Reference for layer and node numbering.

CURRENT ELECTRODES	VOLTAGE ELECTRODES	ΔV_{MAX}
--------------------	--------------------	------------------

Anterior-Anterior

1159	1162	1155	1332	0.450
761	1761	361	1961	0.487

Anterior-Posterior

1605	1761	1005	1362	0.746
405	561	962	1805	0.750
606	1561	605	1361	0.804
806	1561	805	1361	0.809
1405	1561	1005	1362	0.816
605	761	962	1605	0.846
561	1206	961	1806	0.855
561	1406	961	1806	0.871
606	1361	1005	1161	0.871
561	1606	961	1806	0.879
1006	1361	1005	1161	0.885
1206	1361	1161	1205	0.895
606	1161	1161	1205	0.903
806	961	962	1605	0.910
806	1961	405	1361	0.918
761	1206	961	1806	0.919
806	1161	1161	1205	0.924
761	1406	961	1806	0.935
1006	1161	1161	1405	0.943
761	1606	961	1806	0.944
1206	1161	1161	1605	0.957
961	1206	962	1806	0.962
1161	1406	1161	1806	0.966
1161	1205	1162	1405	0.968
1161	1806	1161	1806	0.972
1161	1405	1162	1605	0.975
1010	1163	1163	1402	0.976
961	1406	962	1806	0.977
1161	1605	1162	1805	0.978
1161	1805	1162	1805	0.978
961	1606	961	1806	0.986
961	1806	961	1806	0.989
1163	1402	1163	1603	0.997
1163	1603	1163	1803	1.001
1163	1803	1163	1803	1.002
962	1805	962	1805	1.023
***Eleven layers (962,1805)		962	1805	0.929

(cont'd)

(cont'd)

Side-Side				
700	648	1145	1531	0.464
682	683	1132	1134	0.521
682	883	1332	1344	0.524
1332	1344	1317	1355	0.784
1317	1355	1266	1355	0.843
Anterior-Side				
1266	1355	1034	1355	0.862
1034	1355	1021	1355	0.874
1021	1355	1021	1364	0.879
1021	1364	1010	1163	0.899
Posterior-Posterior/Posterior-Side				
606	1606	161	1833	0.162
1006	1082	1010	1355	0.420

TABLE 5.3 ΔV_{MAX} of various current and voltage electrode locations for the center stomach model.

CURRENT ELECTRODES		VOLTAGE ELECTRODES		ΔV_{MAX}
Anterior-Anterior				
1117	1157	1159	1607	1.32
361	1761	759	1561	1.86
561	1761	960	1760	1.98
361	1561	759	1561	2.00
561	1561	759	1561	2.02
1145	1155	1157	1162	2.16
764	1556	1162	1358	2.34
756	1564	958	1362	2.37
764	1156	1157	1162	2.37
764	1356	1162	1358	2.38
756	1364	958	1362	2.44
958	1564	958	1362	2.44
956	1364	958	1362	2.50
964	1356	1162	1357	2.55
1156	1164	1157	1162	2.60
1158	1361	1158	1361	3.34
1156	1160	1160	1332	3.84
1158	1161	1157	1161	4.17
1157	1161	1157	1161	4.43
Anterior-Posterior				
1205	1360	802	1360	3.07
1005	1360	802	1360	3.07
805	960	1160	1810	3.55
1005	1160	1160	1802	4.26
1160	1802	1160	1810	4.34
1160	1810	1160	1810	4.34
Anterior-Side				
1163	1603	1161	1517	2.675
1010	1163	1161	1332	2.728
Side-Side				
1131	1117	1157	1362	1.33
544	1517	961	1357	1.52

TABLE 5.4 ΔV_{MAX} of various current and voltage electrode locations for the frontal stomach model.

CURRENT ELECTRODES		VOLTAGE ELECTRODES		ΔV_{MAX}
Anterior-Anterior				
804	1204	203	1805	8.050
203	1805	402	1806	16.65
1003	1006	810	1020	16.84
1002	1006	810	1020	19.25
402	1806	401	1807	19.74
Anterior-Side				
917	1006	834	1007	17.94
834	1007	821	1008	22.97
821	1008	810	1020	25.00
Anterior-Posterior				
1159	1005	932	1005	9.052
1358	605	806	1917	9.244
1558	605	806	1917	9.250
1558	805	806	1532	9.690
1358	805	806	1532	9.703
1158	1005	917	1006	10.17
1156	1005	883	1006	12.17
Side-Side				
1049	1048	810	1020	22.95
1010	1020	810	1020	25.44
810	1020	810	1020	26.02

Table 5.5 ΔV_{MAX} of various current and voltage electrode locations for the complete torso model.

CURRENT ELECTRODES		VOLTAGE ELECTRODES		ΔV_{MAX}
Anterior-Anterior				
310	406	83	203	0.637
210	610	2	802	1.446
201	601	2	802	1.566
210	810	1	1002	1.908
202	802	2	1002	2.263
83	203	203	283	2.340
2	802	2	1002	2.356
2	1002	2	1202	2.507
0	1002	1	1003	2.545
2	1202	2	1402	2.585
206	434	205	221	2.600
2	1402	2	1802	2.633
2	1802	2	1802	2.660
0	1003	0	1005	2.784
410	406	206	210	3.032
206	410	206	410	3.050
0	1005	1	806	3.052
0	806	10	806	3.110
10	806	10	606	3.220
10	606	10	606	3.240
210	405	210	406	3.240
206	210	210	406	3.280
210	406	210	406	3.305
Anterior-Posterior				
357	402	157	402	2.464
402	557	357	402	2.462
157	402	157	402	2.465
Side-Side				
434	485	48	201	0.708
448	434	206	210	2.310
Anterior-Side				
317	606	34	404	1.934
517	403	83	403	2.130
83	403	66	403	2.215
66	403	66	403	2.233
203	283	203	483	2.350
434	405	205	221	2.620
205	221	210	405	2.945

Table 5.6 ΔV_{MAX} of various current and voltage electrode locations for corpus contraction analysis in the complete torso model.

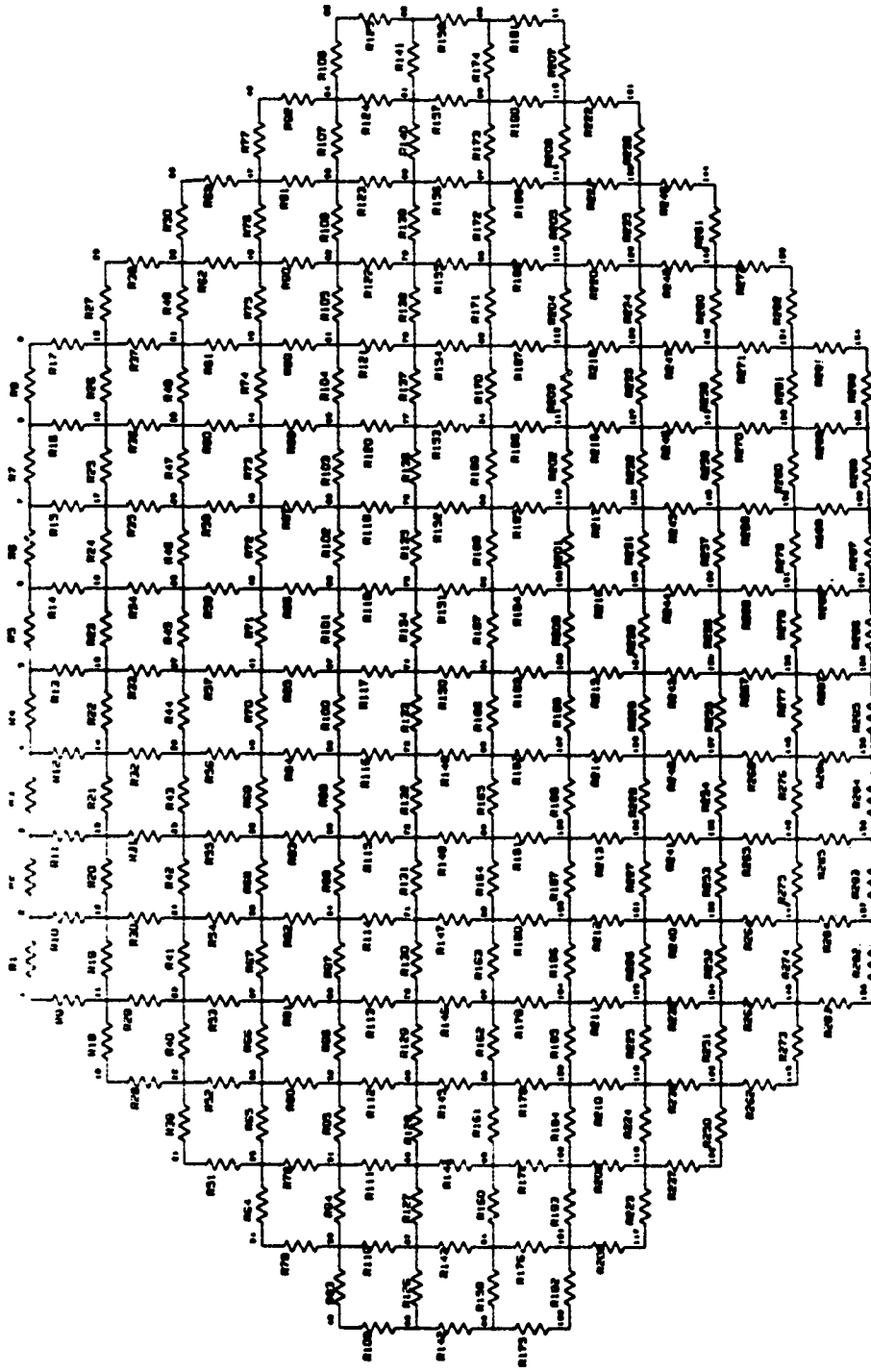


Figure 5.1 Typical layer of the SPICE resistor phantom.

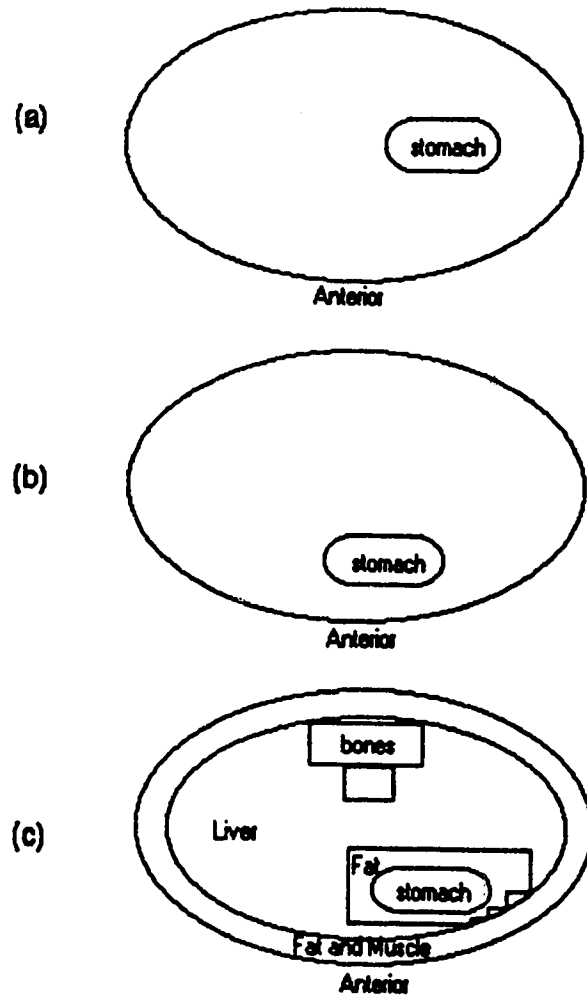


Figure 5.2 Schematic drawings of the three stomach models.
(a) Center stomach model; **(b)** Frontal stomach model;
(c) Complete torso model.

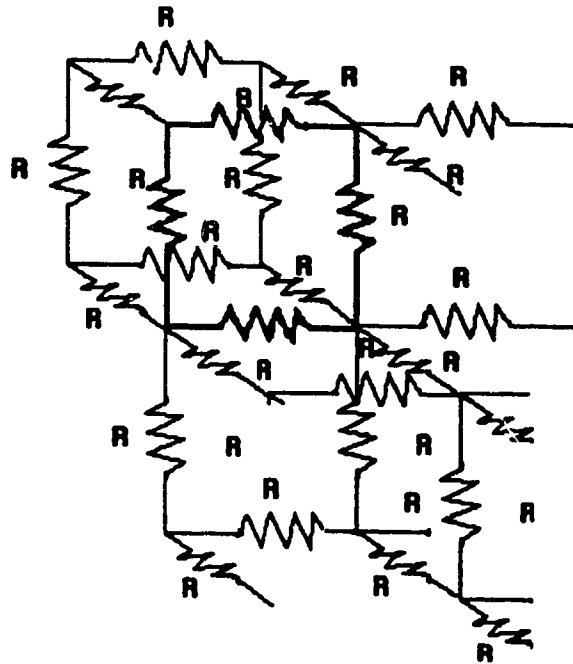


Figure 5.3 Three-dimensional representation of the resistor array. The resistors are interconnected vertically and horizontally forming a lattice.

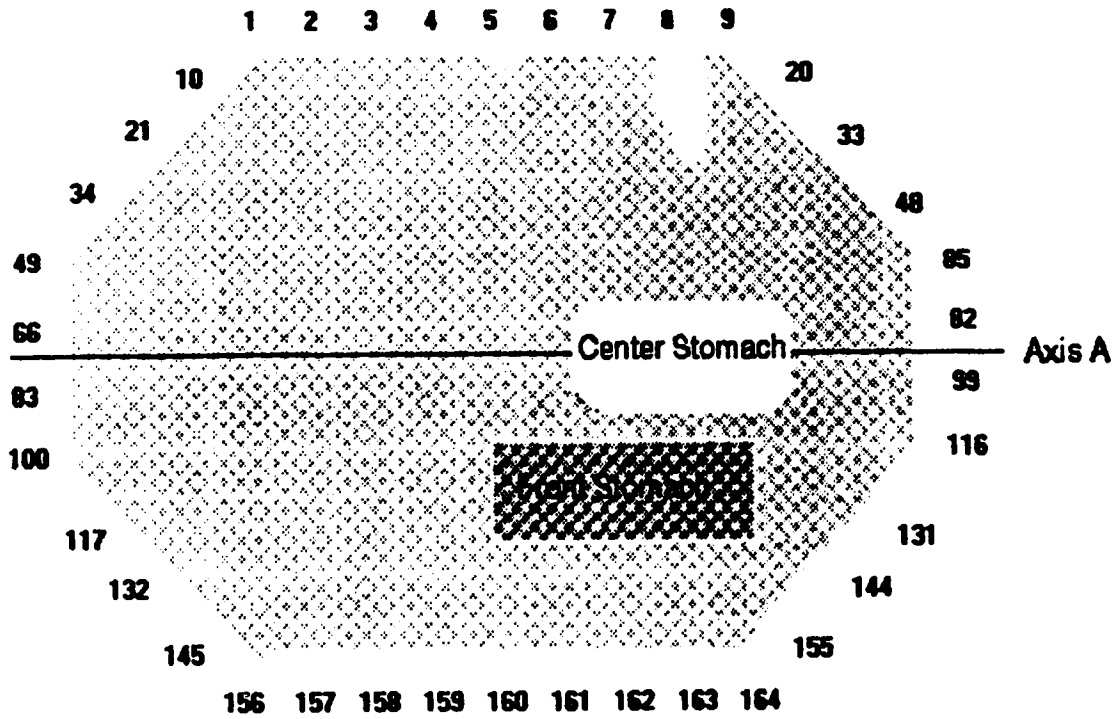


Figure 5.4 Cross section of the resistor phantom for the center stomach model and frontal stomach model. The node numbers for the peripheral of the first layer is also shown.

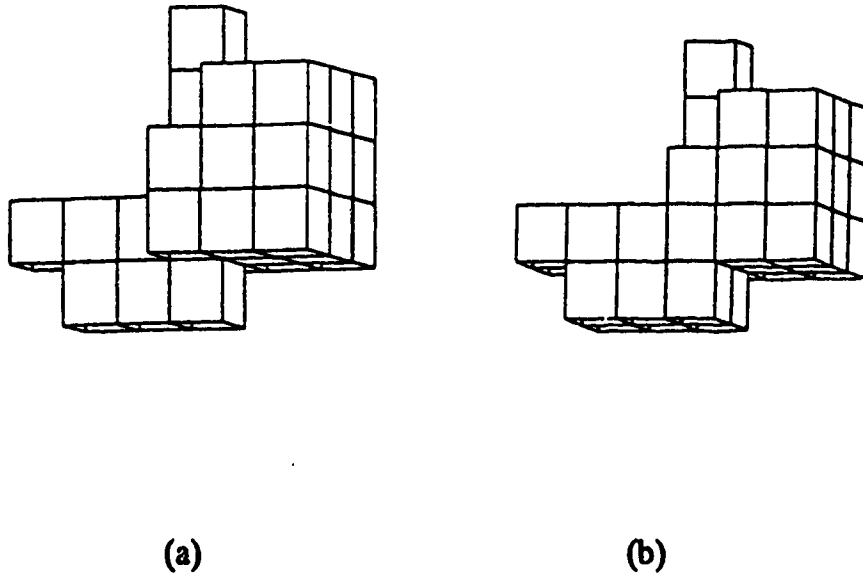
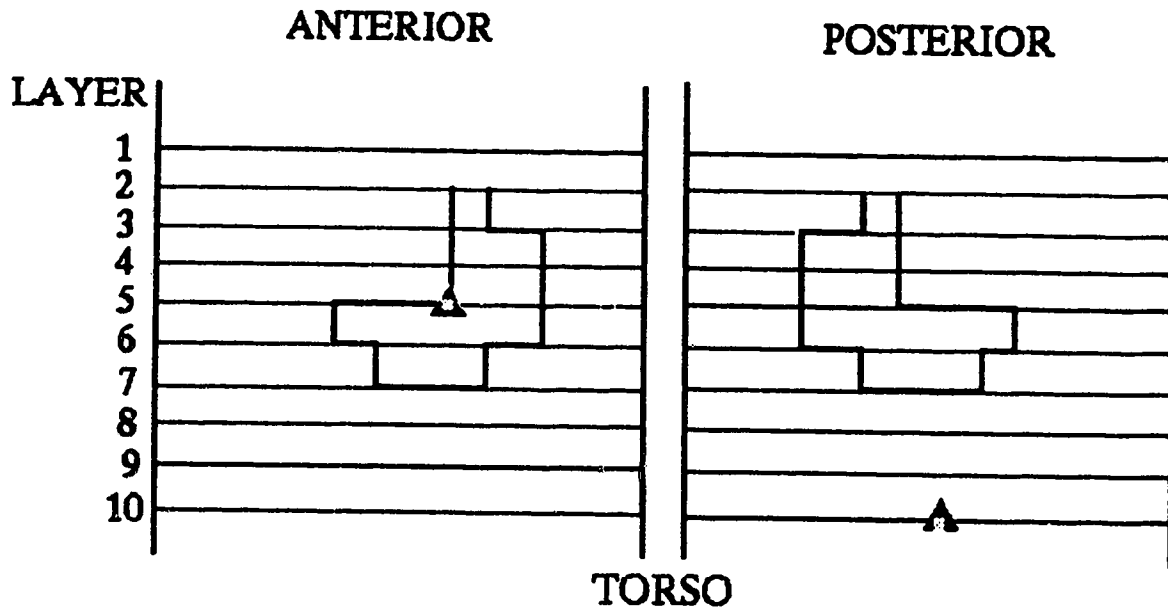


Figure 5.5 Stomach model used in the center stomach model and frontal stomach model analyses.
(a) contracted stomach; **(b)** relaxed stomach.



▲ current electrode
 ■ voltage electrode

Figure 5.6 Optimal electrode locations for the center stomach model analysis.

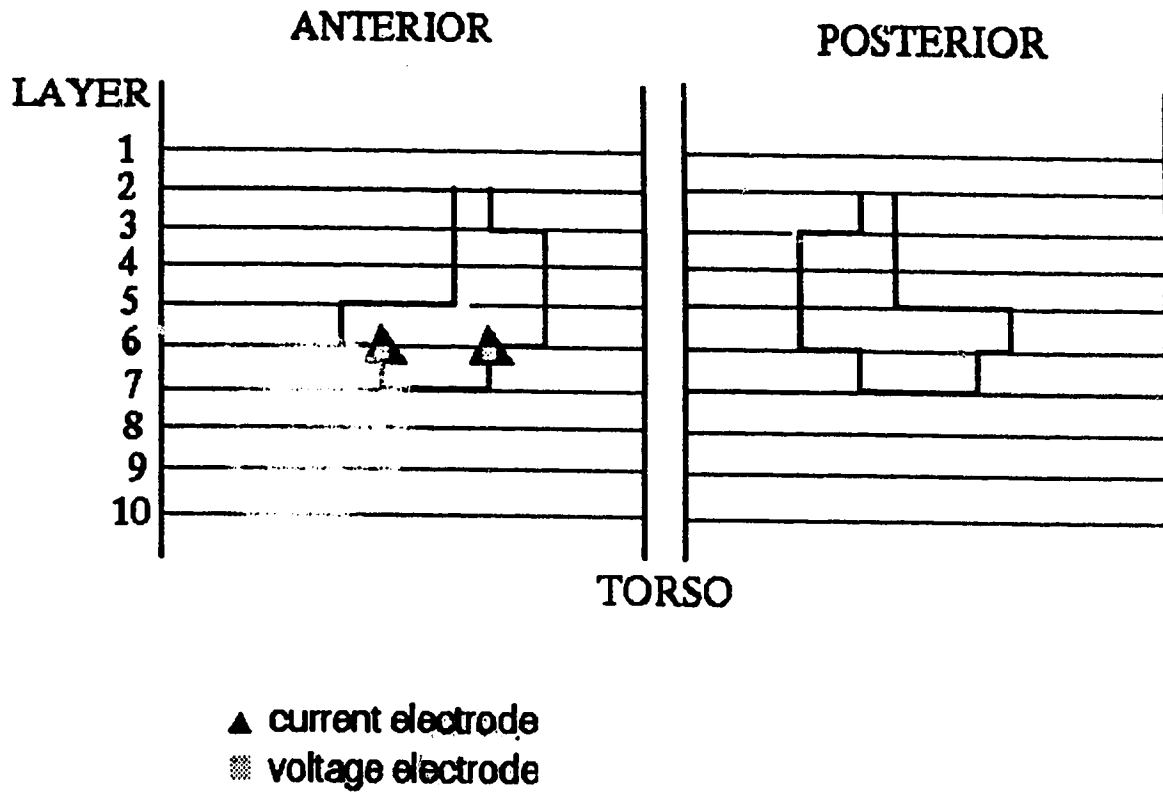


Figure 5.7 Optimal electrode locations for the frontal stomach model analysis.

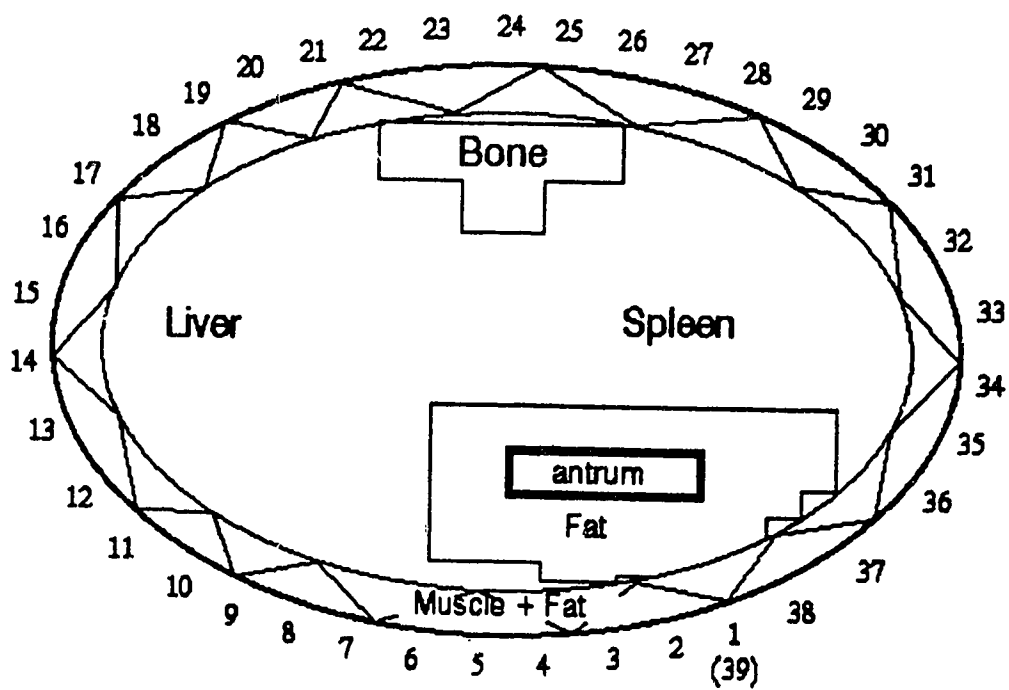


Figure 5.8 A typical cross-section of the resistor phantom at the level of the antrum for the complete torso model analysis.

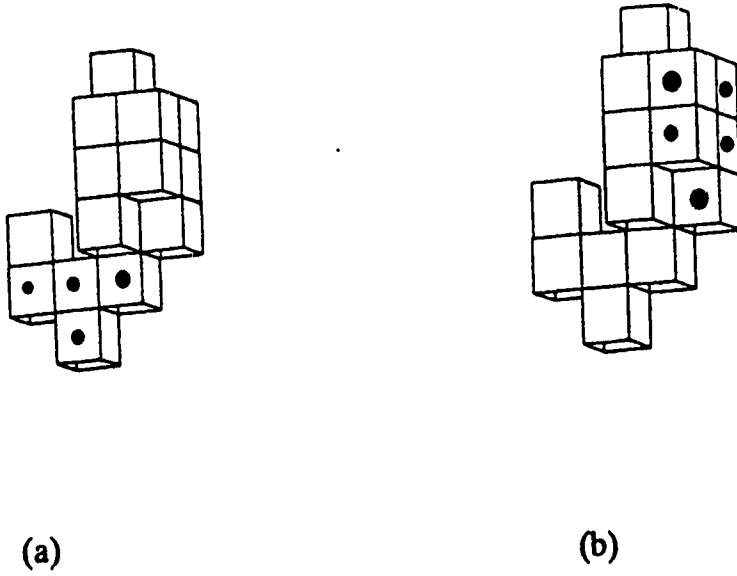


Figure 5.9 Stomach model used in the complete torso model analysis
(a) antral (b) corpus contraction analysis. Contracting
region of each analysis is as marked.

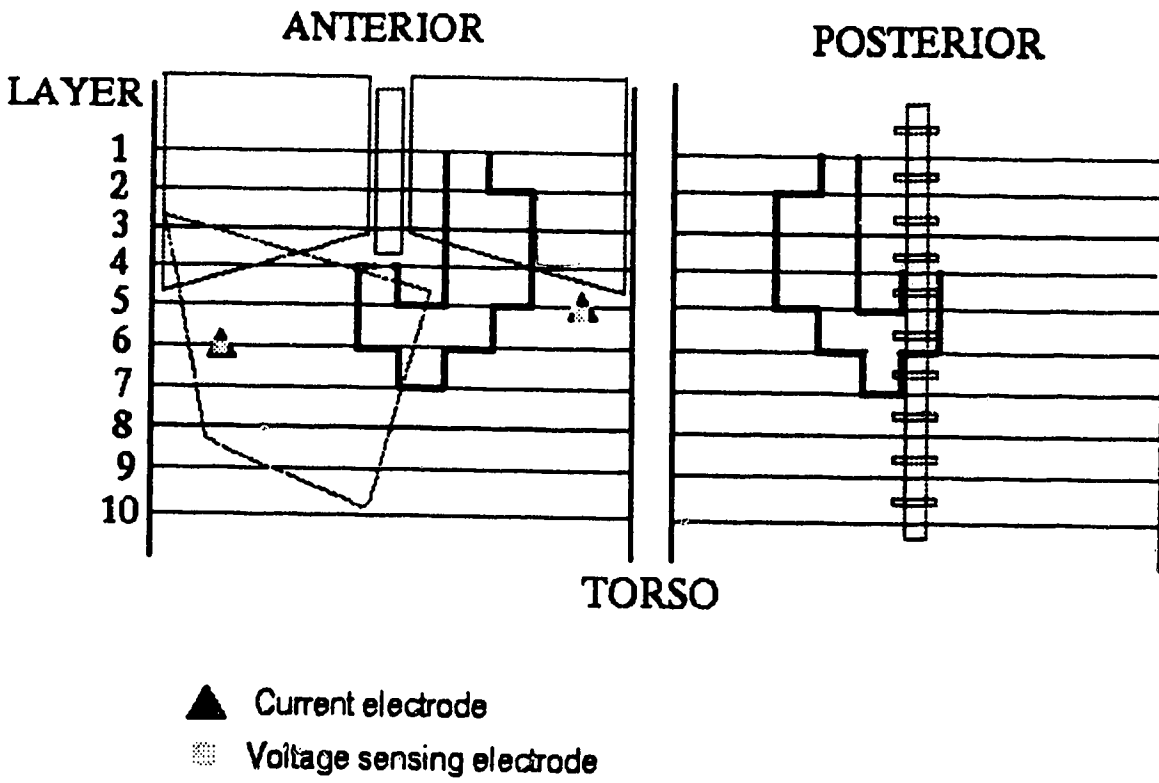


Figure 5.10 Optimal electrode locations for the complete torso model: antral contraction Side- Side analysis.

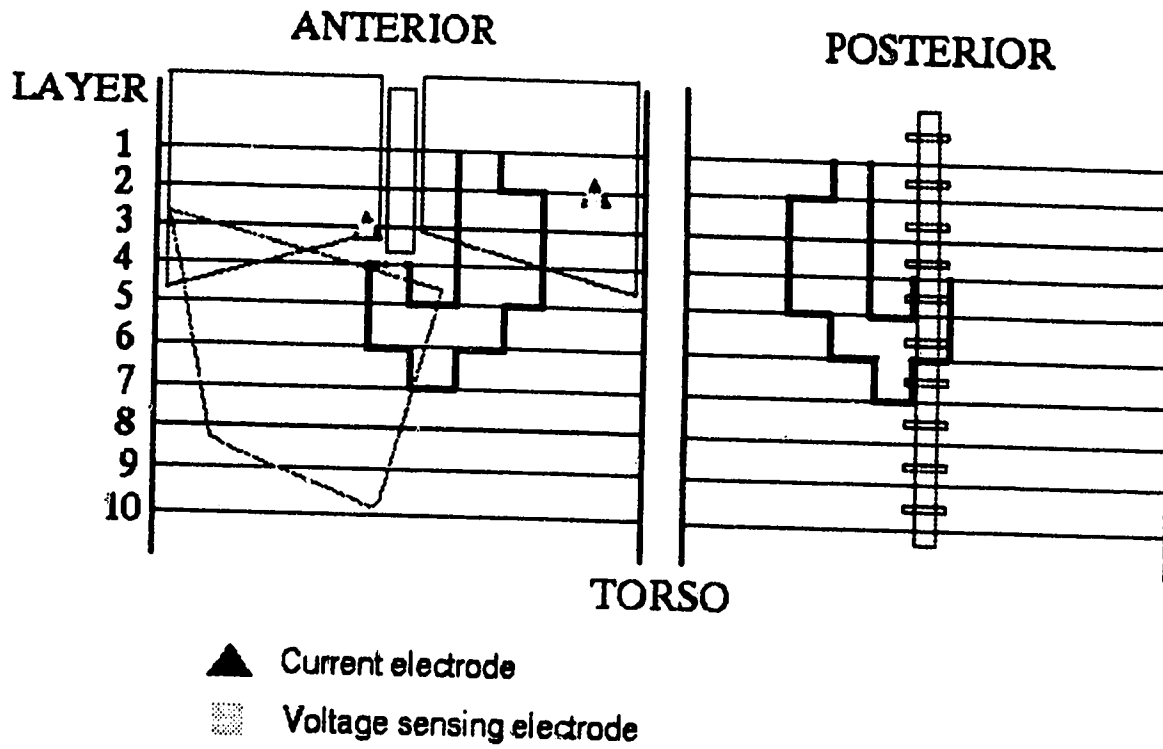


Figure 5.11 Optimal electrode locations for the complete torso model: corpus contraction Anterior-Anterior analysis.

COMPLETE TORSO MODEL - ANTRAL CONTRACTION ANALYSIS

elect1=810; elect2=1020; max= 26.02V; min= 0V

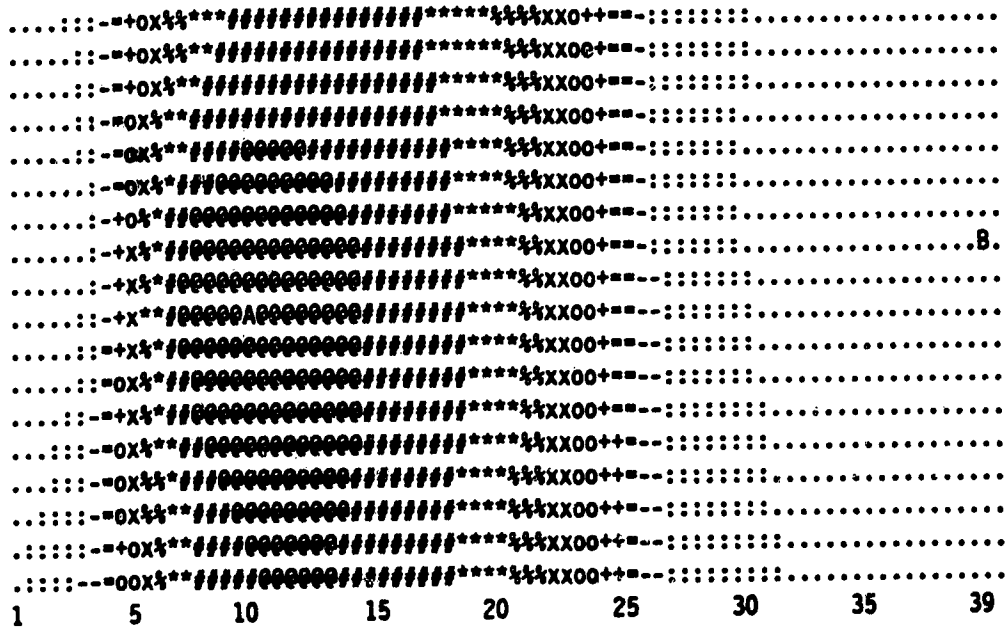


Figure 5.12 Voltage profile on the unwrapped torso for the complete torso model - antral contraction analysis.
 A - current injection electrode, locating on "@"
 B - voltage reference electrode on top of current injection electrode, locating on "."
 The voltage profile is formed by measuring the absolute change in potential difference on the torso surface with respect to the reference electrode.
 The Relative voltage magnitude in ascending order is:
 . : - = + o x % * # @

VI. EXPERIMENTAL VALIDATION OF THE 3-D SPICE MODEL

6.1 INTRODUCTION

After the intensive study of the three-dimensional SPICE model, the optimal electrode locations for the tetra-polar electrode configuration have been found, as shown on FIG.5.10 and FIG.5.12. The results suggest that the standard anterior-posterior electrode placement used in IE, suggested by McClelland and Sutton(1985), as shown on FIG.4.6, may not provide the best possible IE recordings for the analysis of gastric contractile activity, although it has been found to measure gastric emptying successfully. From simulations using the SPICE model, the results indicate that the best locations for the measurement of impedance variations is to have all four electrodes on the anterior side of the torso. In order to validate the new scheme of electrode placement suggested by the SPICE model, two sets of experiments were done. The first experiment was to compare the strength of gastric contractile IE signals measured with the two electrode placement schemes. The second experiment was conducted to validate that the IE signals recorded with SPICE electrode scheme was actually the gastric activity.

The impedance monitoring device used in the experiments was designed by Familoni(1986). A schematic of the circuitry is shown in FIG.6.1. The device applies a current of 4mA peak to peak at 100kHz through two current electrodes to the torso and two voltage electrodes

measure the potential difference across the torso. The recorded signal may include blood flow in the region under the electrodes, volume variations from respiration, gastric contractile activity and motion artifacts.

Before the experiment, the volunteers were asked to fast for eight hours. The subject assumed the supine position during the experiment. The skin around the torso was abraded and then treated with alcohol to reduce electrode motion artifacts. Adhesive Ag/AgCl electrodes (for ECG) were then placed at various locations. While recording, the subject was asked to remain as motionless as possible. IE and respiration were recorded with two separate channels.

6.2 SPICE ELECTRODE PLACEMENT VS STANDARD ELECTRODE PLACEMENT

6.2.1 Procedures

Two volunteers were involved in this test. In the first 20 minutes, the gastric impedance was monitored with the SPICE electrode placement. In the next 20 minutes, it was monitored with the standard electrode placement. The subjects were then given 100g ground beef, 100g fried potatoes and 100ml orange juice. The gastric impedance was then monitored for 45 minutes with the SPICE electrode placement. Afterwards, the subject was given the same meal and gastric impedance was monitored with the standard electrode placement for another 45 minutes.

6.2.2 Results and Discussion

The results from the two volunteers measured with the two electrode placement schemes before and after the ingestion of food are shown in FIG.6.2 to FIG.6.5. FIG.6.2 and FIG.6.4(a)(b) contain the recordings from volunteers A and B respectively. The results indicate that the amplitude of the signal increases after ingestion. After band-pass filtering, the increase is more apparent, as shown in FIG.6.3, FIG.6.5(a)(b). This increase is as expected. After ingestion, the gastric activity should be higher and hence more contractile activity should be recorded. Also, if the IE has actually recorded the gastric contractile activity, the increase in signal amplitude should be accompanied by the increase in the 3cpm signal. The frequency spectrum of the signals from volunteers A and B are given in FIG.6.6 and FIG.6.7 respectively. After ingestion, the SPICE scheme shows the distinctive 3cpm(0.05Hz) signal from both volunteers. However, the standard scheme shows the 3cpm signal from only volunteer B. Also, the power spectrum of the SPICE scheme is purer than it is from the standard scheme. Therefore, the 3cpm signal is more apparent in the recordings with the SPICE scheme. The power spectral arrays (PSA) of the signals are shown on FIG.6.8a and FIG.6.8b. This function is sensitive to the periodicity within a signal (Challis and Kitney, 1990). The PSA of the recordings from the SPICE scheme, after ingestion, shows the 3cpm periodicity in both volunteers. The PSA of the standard scheme shows the 3cpm periodicity in volunteer B only.

Overall, the amplitude of the 3cpm signal recorded using the SPICE scheme is higher and more evident than using the standard scheme. In the frequency domain, the power spectrum is purer and the 3cpm signal more distinctive in the former than in the latter.

6.3 IE SIGNAL VALIDATION WITH THE EGG

6.3.1 Procedures

The experimental setup for experiment B was similar to experiment A. The position of volunteer C was the same as in experiment A. In this experiment, the EGG was also monitored. FIG.6.9 shows the locations of all the electrodes used. There were six channels of recording during the experiment; channel one was respiration; channel two was IE and channels three to six were the EGG. Measurements were made for 1½ hours during the fasting state. In the next 2 hours, volunteer C was given 200g ground beef, 150g fried potatoes and 150ml orange juice. The EGG and IE were then recorded.

6.3.2 Results and Discussion

In the following discussions, only channel 5 of the EGG will be used to correlate to the IE. Qualitatively, the other three EGG channels were similar to channel 5.

6.3.2.1 Before ingestion

The recordings in the fasting state are shown in FIG.6.10(a-c). Before ingestion, the IE showed momentary contractile activity. In the intervals 55-65, 70-77 and 80-90 minutes, the IE showed strong contractile activity. The EGG also increased in amplitude after the 50th minute. Although the increase in EGG activity does not always imply an increase in contractile activity, the increase in IE signal amplitude was correlated with the increase in EGG amplitude. This is a good indication that the IE is sensitive to the 3cpm gastric contractile activity. In fact, the EGG is always present whether or not there is contractile activity. Also, the time frequency plot of the IE overlaps that of the EGG at the 8-10, 55-60, 68-85 minute intervals, as shown in FIG.6.11. This implies that they are synchronous at these intervals. Since gastric contractions are synchronous with the EGG, it suggests that the IE is sensitive to the contractile activity during these intervals. Since this activity is recorded in the interdigestive phase of the stomach, the IE may have recorded the phasic behavior of the migrating motility complex (the MMC). The cross-spectral array between IE and EGG is shown in FIG.6.12. This figure also shows the phasic behavior of the MMC.

6.3.2.2 After ingestion

The signals recorded after ingestion were also analyzed as described in the previous section. The amplitude of the IE and the EGG is increased, as shown in FIG.6.13(a-c). Both the IE and EGG show strong activity during most of the interval shown. This indicates

that the IE and the EGG are sensitive to the expected gastric activity after ingestion. Weaker phases appear at the 40-50, 70-90 and 110-120 minute intervals. Also, the activity of the IE and EGG signals seems to be correlated. This again is a good indication that the IE is recording the gastric contractile activity. From the time frequency plot on FIG.6.11, the IE recording is synchronized to the EGG for most of the interval shown except during the 43-52 minute and the 73-85 minute intervals. This can also be seen from the PSA of FIG.6.14. The cross spectral array (CSR) indicates the shift in frequency occurred at the 48th minute, as shown in FIG.6.15. The two quiet phases occur between 32-48 minute and 67-80 minute indicate that the gastric contractile activity is low.

6.4 CONCLUSIONS

From experiment B, since the IE signals recorded from the SPICE electrode placement scheme show very high correlation with the EGG, one might conclude that the 3cpm signals recorded by the SPICE scheme is the gastric contractile activity. However, to confirm that the SPICE IE electrodes are measuring actual gastric contractions, it would be necessary to implant force transducers onto the muscular lining of the stomach. Results in experiment A suggest that the SPICE electrode placement scheme records better IE signals than the standard electrode placement scheme. The former measures more gastric contractile activity than the latter. The 3cpm (0.05Hz) signal is observable in the time domain and is distinct in the power spectrum.

In view of the above, the conclusions are:

- a) the three dimensional SPICE model has reasonably modelled the torso and the stomach contractile activity; it has basically solved the problem of the 2-dimensional modelling of a 3-dimensional system; the SPICE model has provided the optimal electrode locations for the monitoring of the antral contractile activity; experimentally, the optimal electrode placement is as shown on FIG.6.10;**
- b) the SPICE electrode placement scheme records more of the epigastric impedance signal than the standard tetra-polar electrode placement used by McClelland and Sutton(1985);**
- c) the new electrode placement scheme is useful for IE to monitor the gastric contractile activity together with the EGG; the inexpensive and non-invasive nature of IE might make it a better choice for monitoring gastric motility.**

6.5 SUGGESTIONS FOR FUTURE RESEARCH

The 3-dimensional SPICE model can theoretically model any resistive system. Therefore, the model can be used to model other biological systems or to determine and investigate the image reconstruction algorithms for APT. The remaining problem will be the availability of computer memory and the time required for performing the simulations. One may attempt a more accurate modelling with

more resistors in each layer and increase the number of layers in the model so that more biological factors may be included, for example, the effects of the respiratory system and the circulatory system.

IE with the new electrode scheme can record gastric contractile activity; nevertheless, further study on the reliability is required. For diagnostic purposes, the IE wave shape, the variation of amplitude and frequency, and also the correlation with the EGG, should all be investigated.

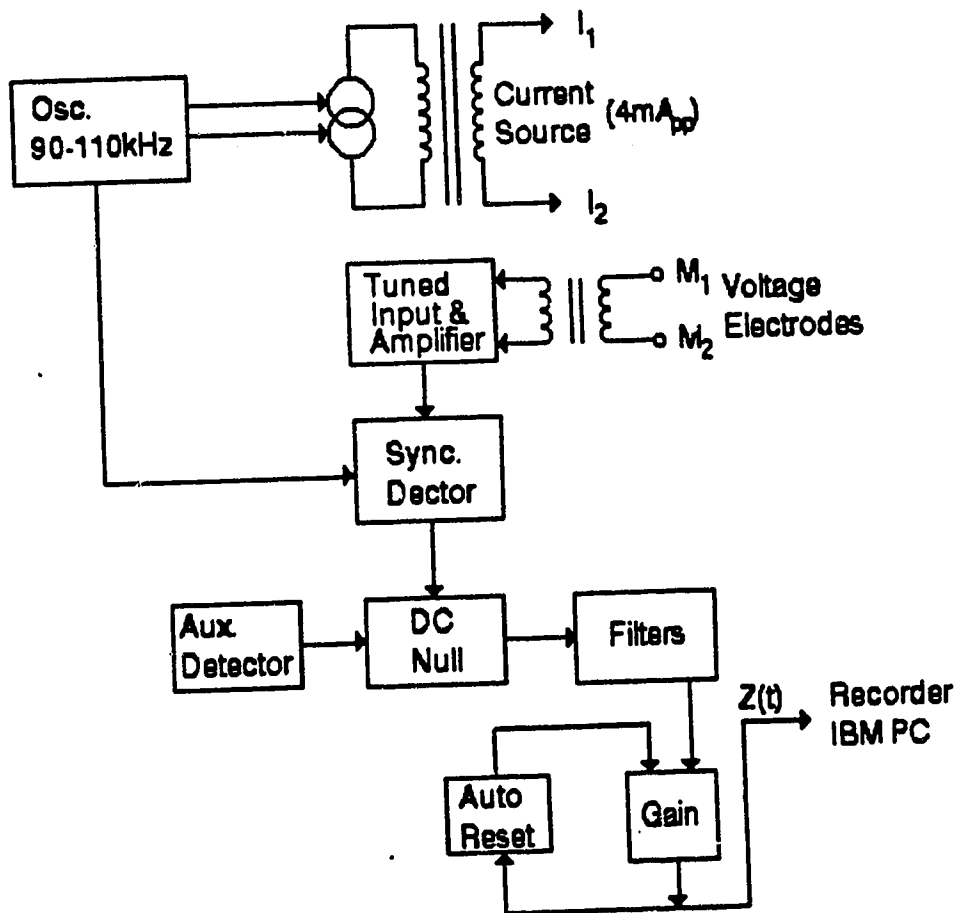


Figure 6.1 Schematic Diagram of the Impedance Monitoring Device. (adapted from Familoni, 1986)

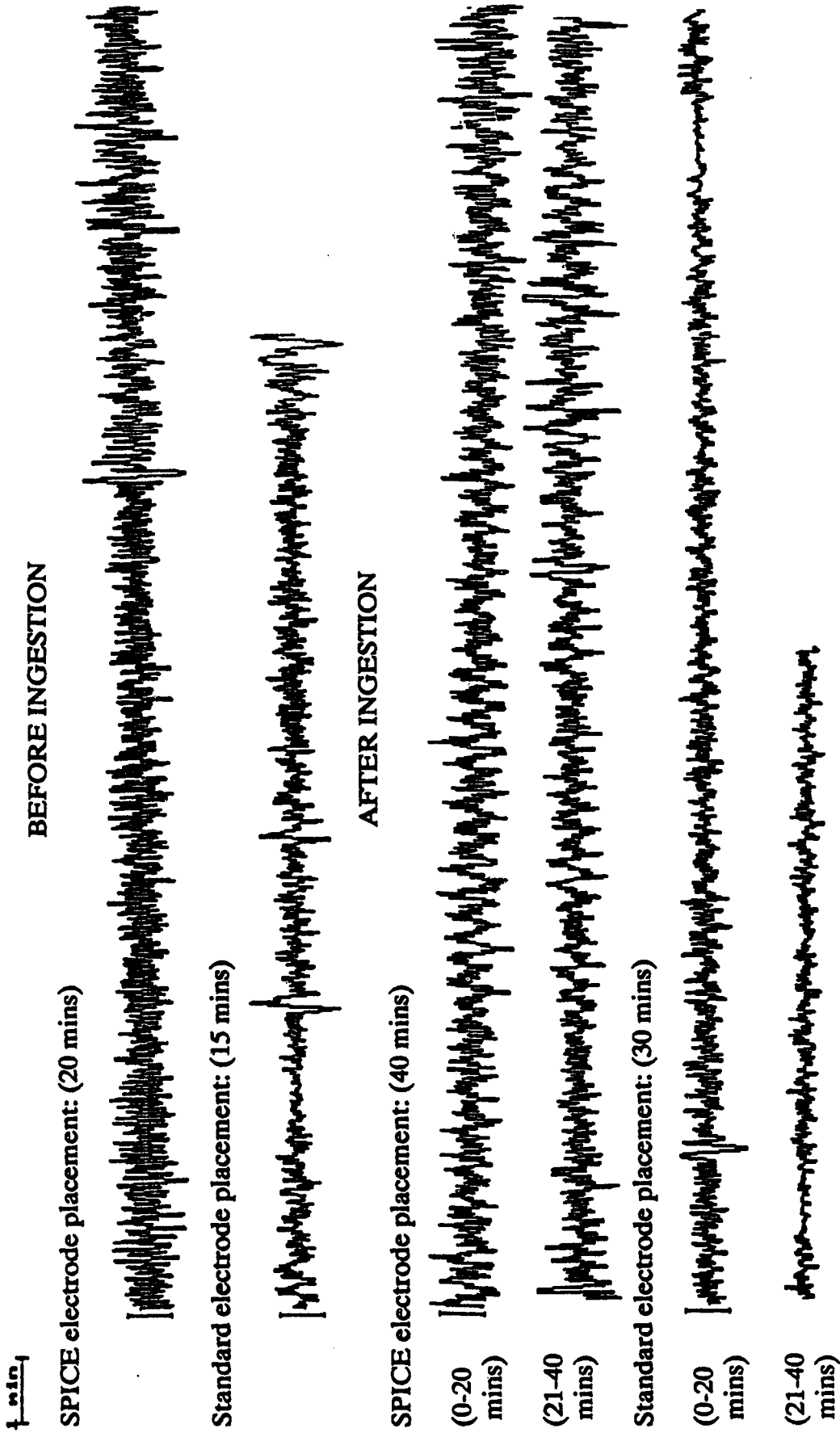


Figure 6.2 Recordings of IE with SPICE electrode placement and Standard electrode placement. (Volunteer A)

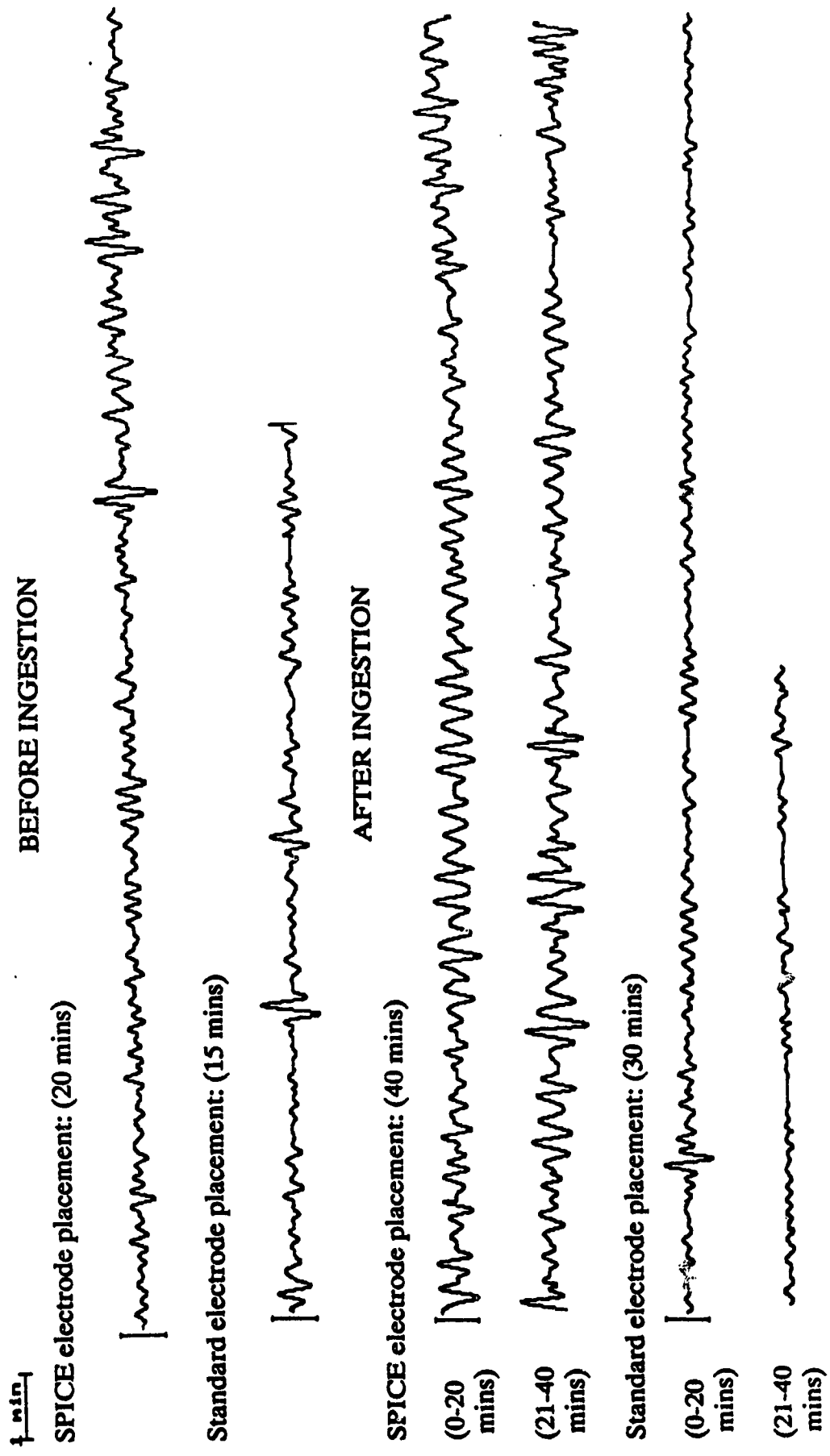


Figure 6.3 Recordings of IE after digital bandpass filtering (0.02Hz - 0.1Hz).
Volunteer A

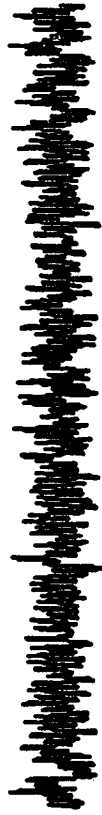
BEFORE INGESTION

$\frac{1 \text{ min}}{\text{-----}}$

SPICE electrode placement: (30 mins)



(0-20 mins)



(21-30 mins)

Standard electrode placement: (20 mins)

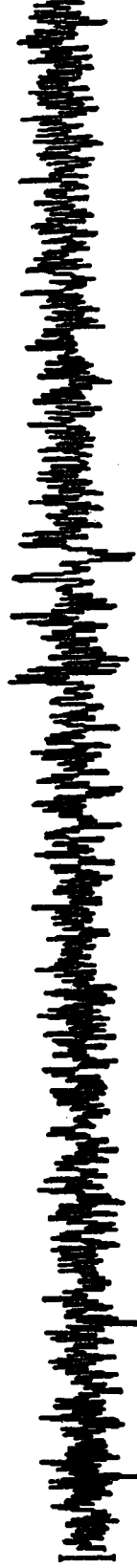
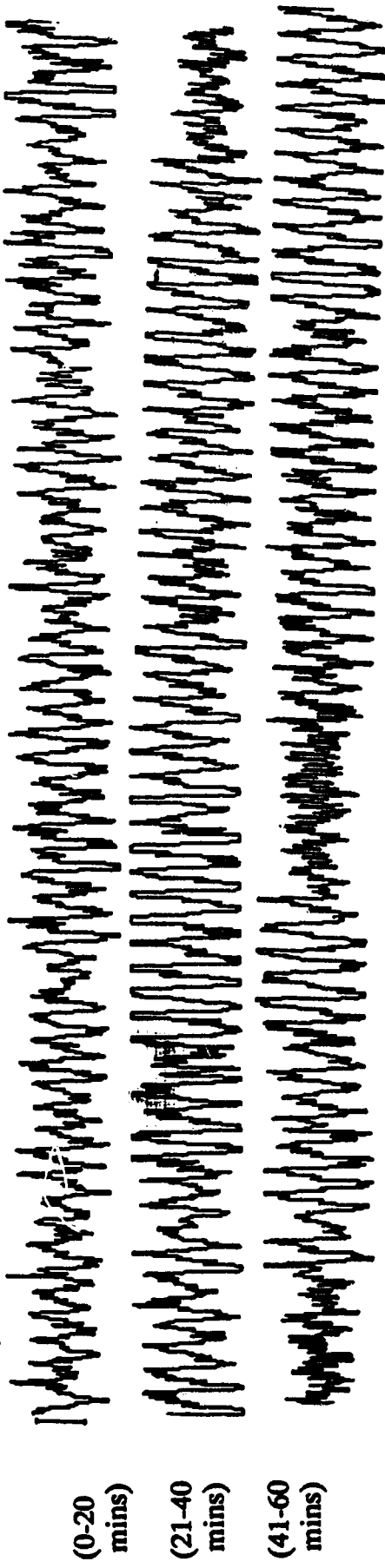


Figure 6.4a Recordings of IE before ingestion.
(Volunteer B)

AFTER INGESTION

1 min

SPICE electrode placement: (60 mins)



Standard electrode placement: (40 mins)

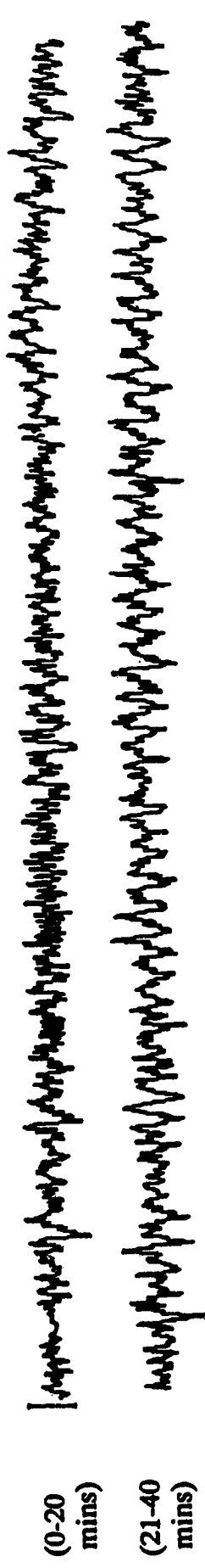


Figure 6.4b Recordings of IE after ingestion.
(Volunteer B)

BEFORE INGESTION

↑ 1 min ↓

SPICE electrode placement: (30 mins)



88

Standard electrode placement: (20 mins)

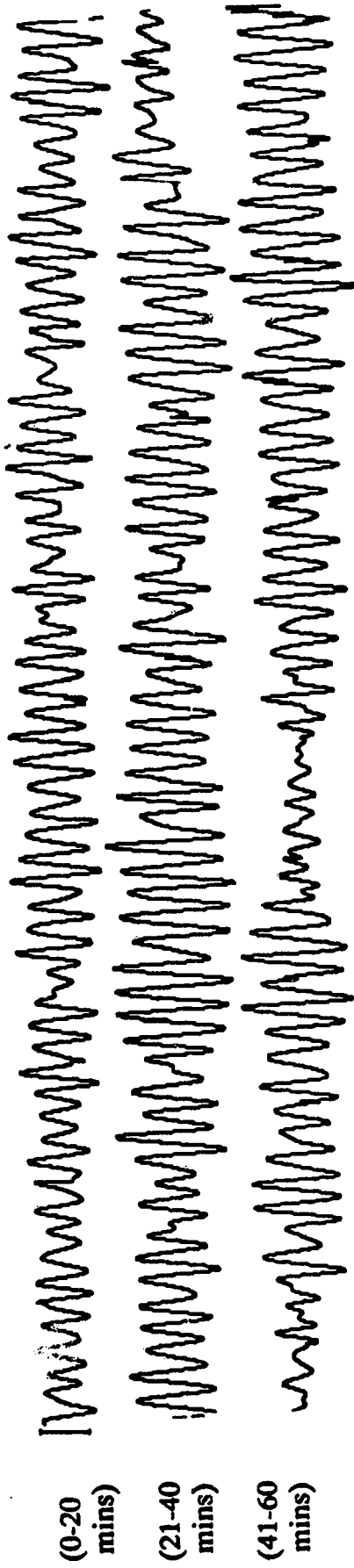


Figure 6.5a Recordings of IE before ingestion, after bandpass filtering (0.02Hz-0.1Hz).
(Volunteer B)

AFTER INGESTION

1 min

SPICE electrode placement: (60 mins)



Standard electrode placement: (40 mins)

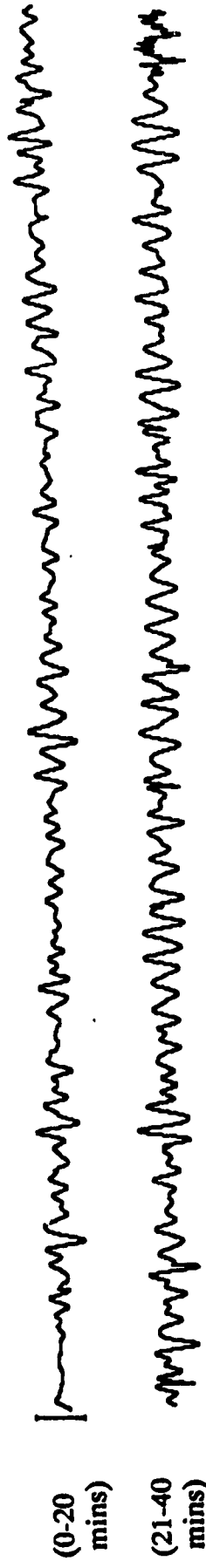


Figure 6.5b Recordings of IE after ingestion, after bandpass filtering (0.02Hz-0.1Hz). (Volunteer B)

Volunteer A

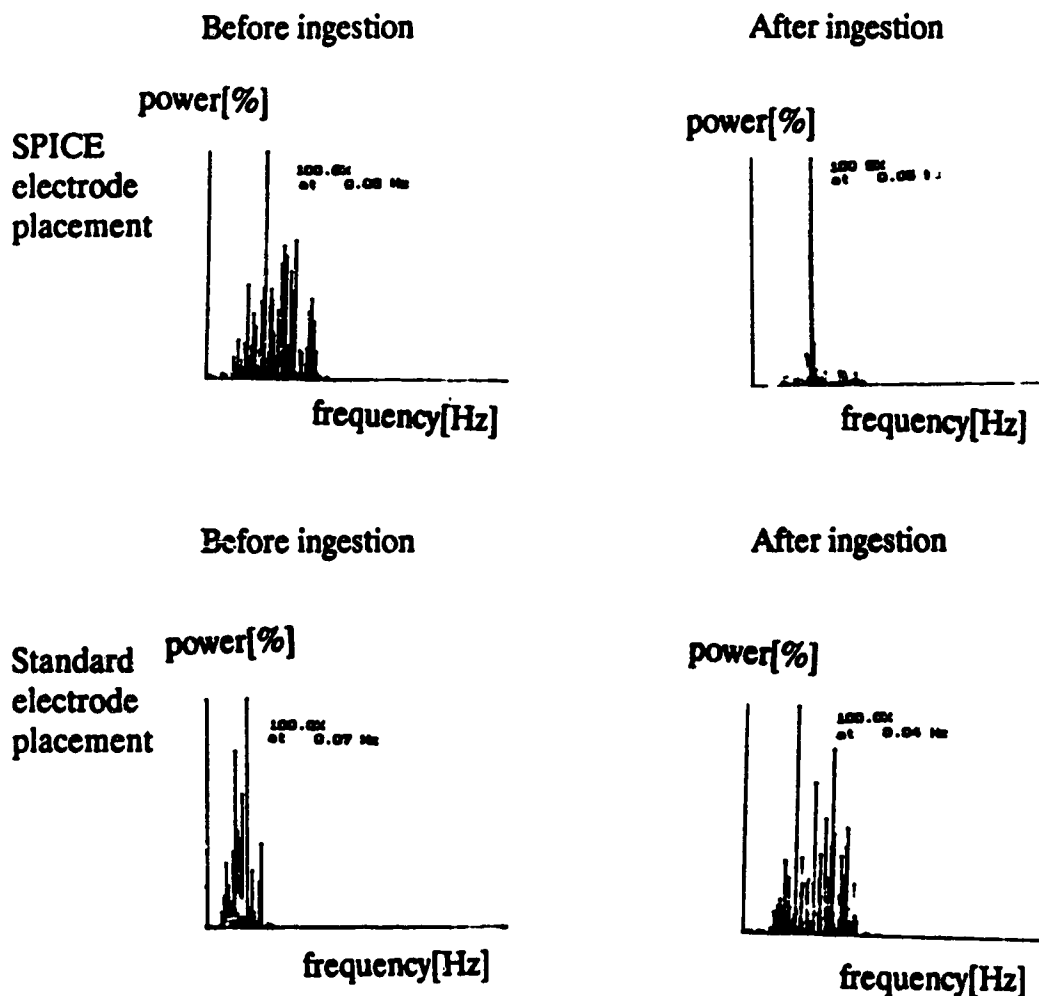


Figure 6.6 Frequency spectrum of the IE from experiment A.

Volunteer B

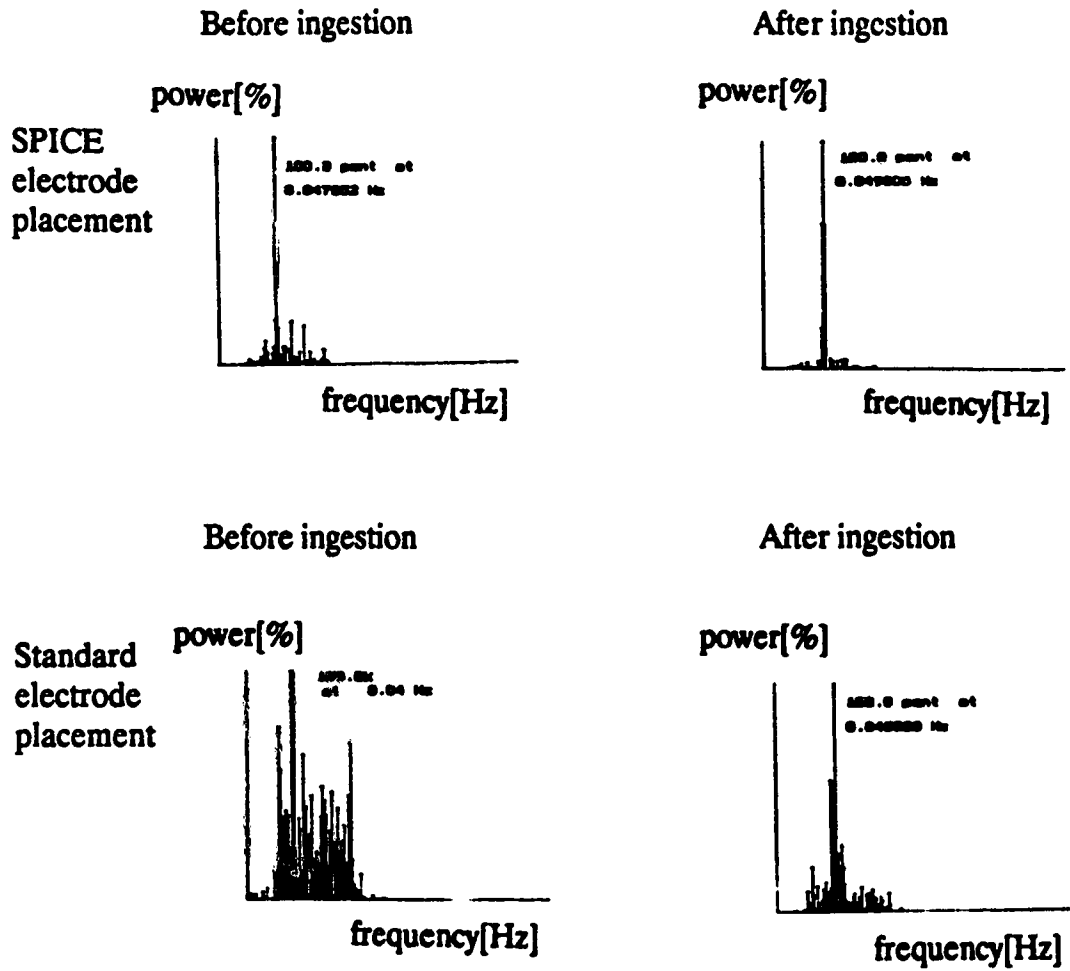
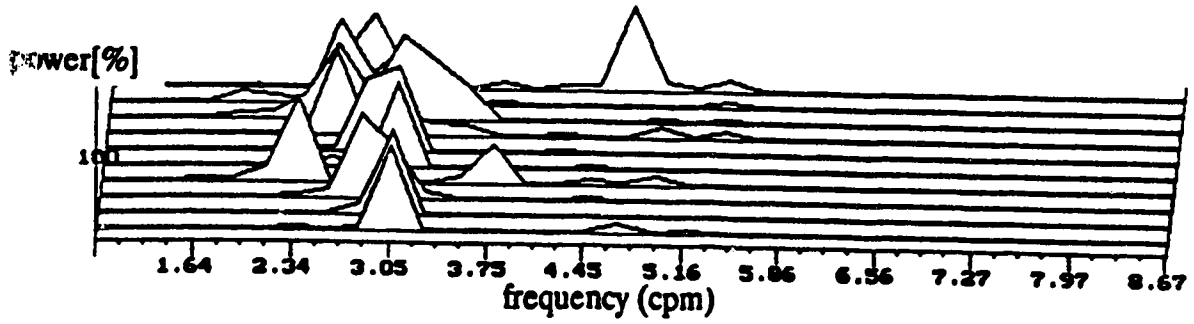


Figure 6.7 Frequency spectrum of the IE from experiment A. (Volunteer B)

Volunteer A

SPICE electrode placement

After ingestion: (time step - 4.27 mins)



Standard electrode placement

After ingestion: (time step - 4.27 mins)

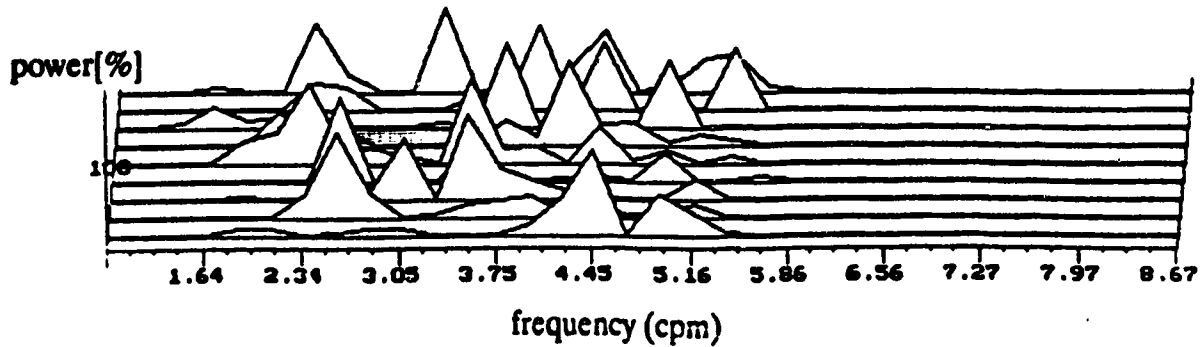
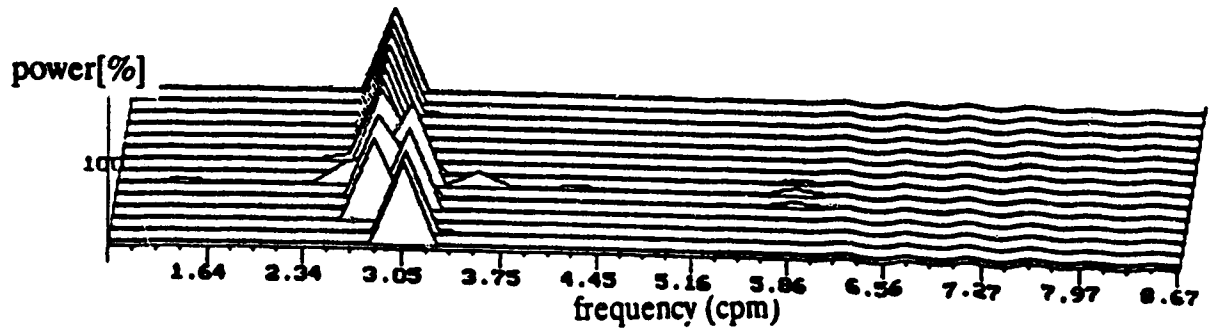


Figure 6.8a Power spectra arrays of recordings from Volunteer A.

Volunteer B

SPICE electrode placement

After ingestion: (time step - 4.27 mins)



Standard electrode placement

After ingestion: (time step - 4.27 mins)

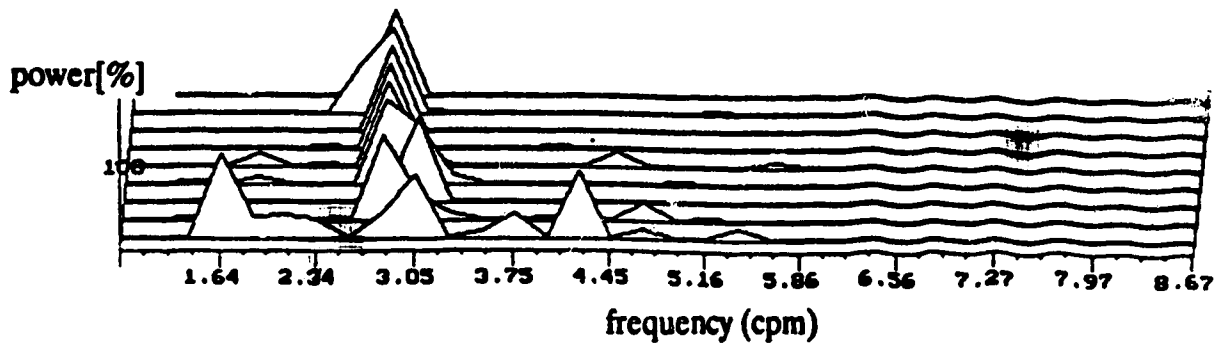
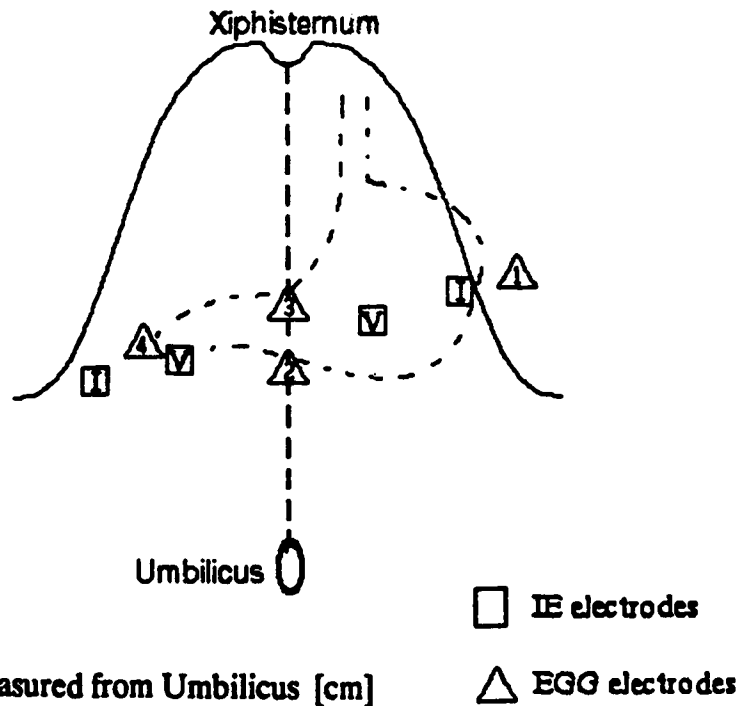


Figure 6.8b Power spectral arrays of recordings from Volunteer B.



Measured from Umbilicus [cm]

Xiphisternum (0,21)

IE electrode locations:

I: (4.45, 11.5); (-6.5, 8.25)

V: (1.85, 10.75); (-3.5, 9)

EGG electrode locations:

1 (7, 12.5)

2 (0, 9)

3 (0, 11.5)

4 (-3.75, 10.5)

ground (left hip)

EGG

electrodes	channel
(1, 2)	3
(1, 3)	4
(1, 4)	5
(3, 4)	6

Figure 6.9 Location of EGG electrodes and IE electrodes in Experiment B.

Volunteer C

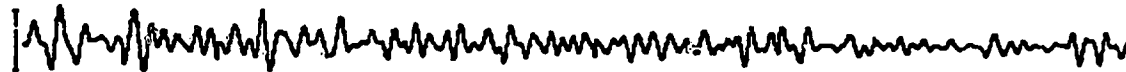
(0-20 mins)

1 min

(i)



(ii)



(iii)



(20-40 mins)

(i)



(ii)



(iii)



Figure 6.10a IE and EKG of Experiment B, before ingestion (0-40 mins).
(i) IE; (ii) IE after bandpass filtering; (iii) EKG channel 5.
(Volunteer C)

Volunteer C

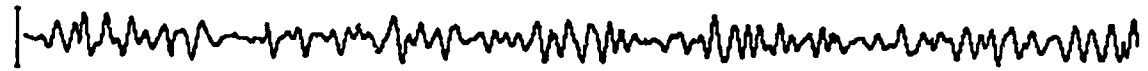
(40-60 mins)

1 min

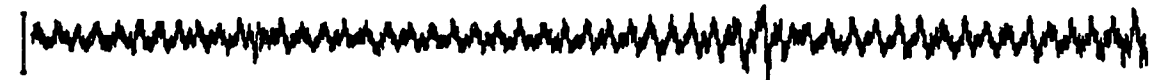
(i)



(ii)

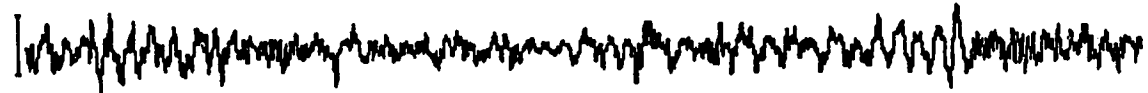


(iii)



(60-80 mins)

(i)



(ii)



(iii)



Figure 6.10b IE and EGG of Experiment B, before ingestion (40-80 mins).
(i) IE; (ii) IE after bandpass filtering; (iii) EGG channel 5.
(Volunteer C)

Volunteer C

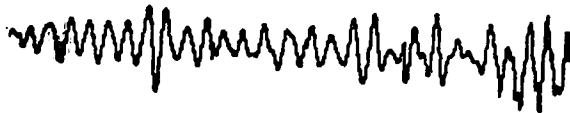
(80-90 mins)

1 min

(i)



(ii)



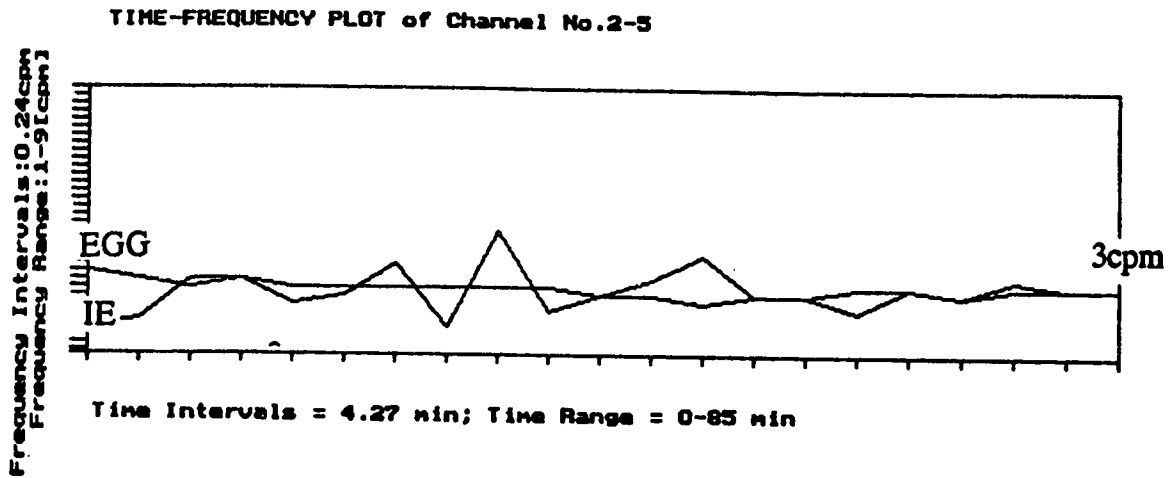
(iii)



Figure 6.10c IE and EGG of Experiment B, before ingestion (80-90 mins).
(i) IE; (ii) IE after bandpass filtering; (iii) EGG channel 5.
(Volunteer C)

Volunteer C

Before ingestion:



After ingestion:

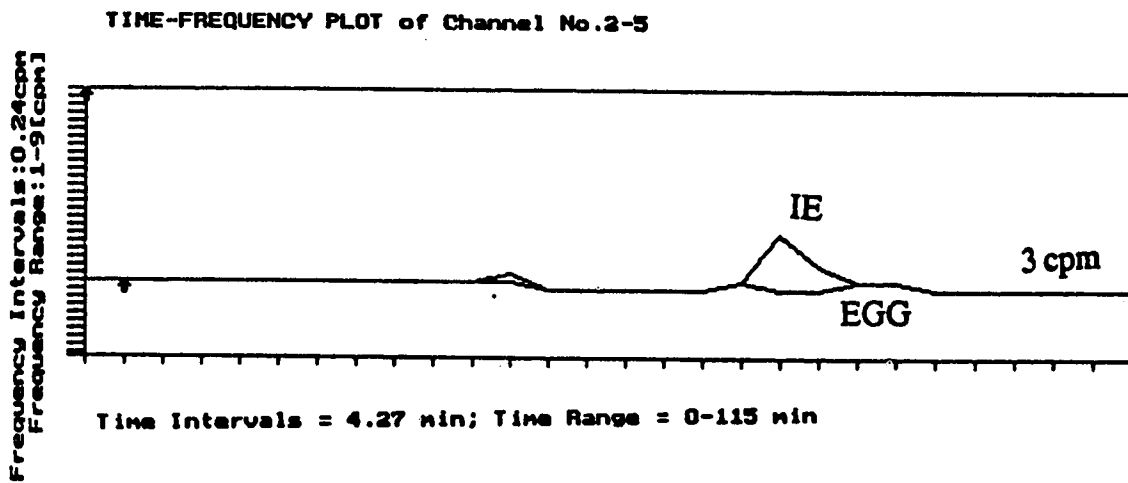
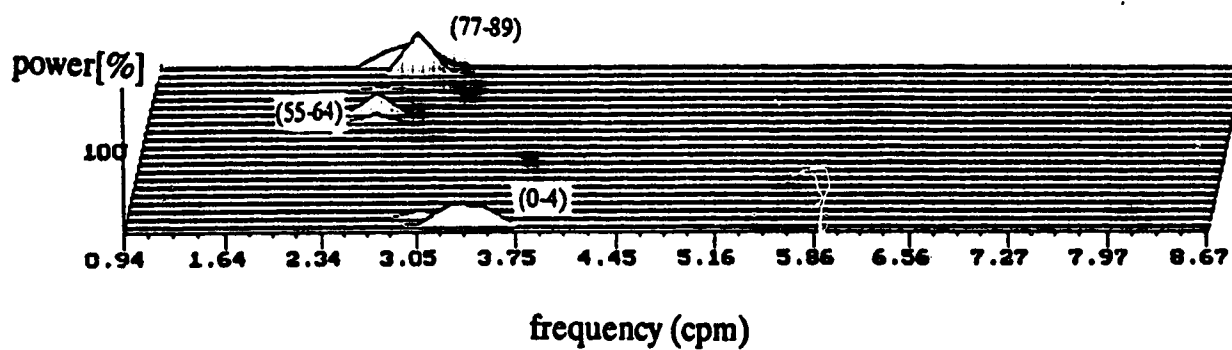


Figure 6.11 Time-Frequency Plot of IE and EGG before and after ingestion.

Volunteer C

**Cross-spectral array between IE and EGG:
(total time: 0 - 89.6 mins; time step: 4.27 mins)**



**Figure 6.12 Cross-spectral array between IE and EGG.
(before ingestion; Volunteer C)**

Volunteer C

(0-20 mins)

1 min

(i)



(ii)



(iii)



(20-40 mins)

(i)



(ii)



(iii)

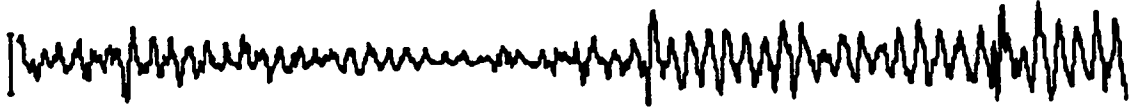


Figure 6.13a IE and EGG of Experiment B, after ingestion (0-40 mins).
(i) IE; (ii) IE after bandpass filtering; (iii) EGG channel 5.
(Volunteer C)

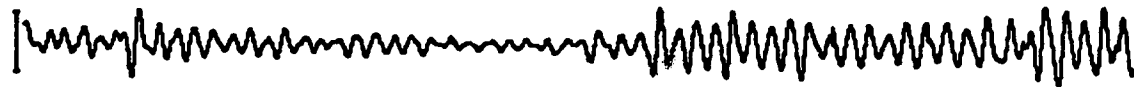
Volunteer C

(40-60 mins)

(i)



(ii)

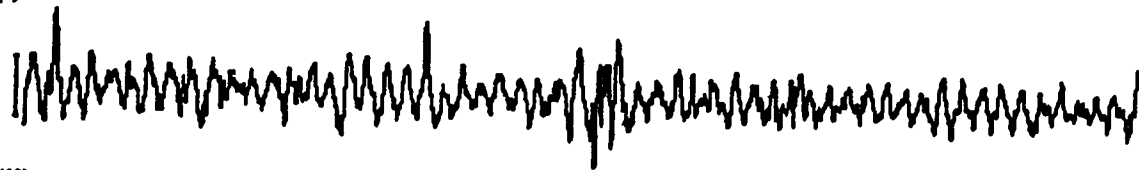


(iii)



(60-80 mins)

(i)



(ii)



(iii)

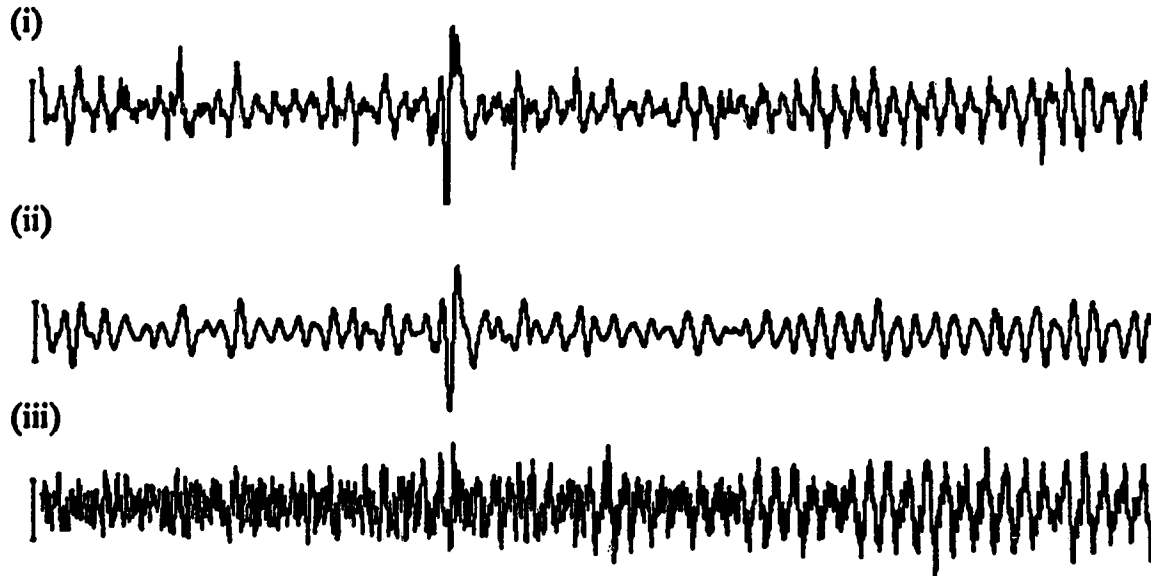


Figure 6.13b IE and EGG of Experiment B, after ingestion (40-80 mins).
(i) IE; (ii) IE after bandpass filtering; (iii) EGG channel 5.
(Volunteer C)

Volunteer C

(80-100 mins)

1 min



(100-120 mins)

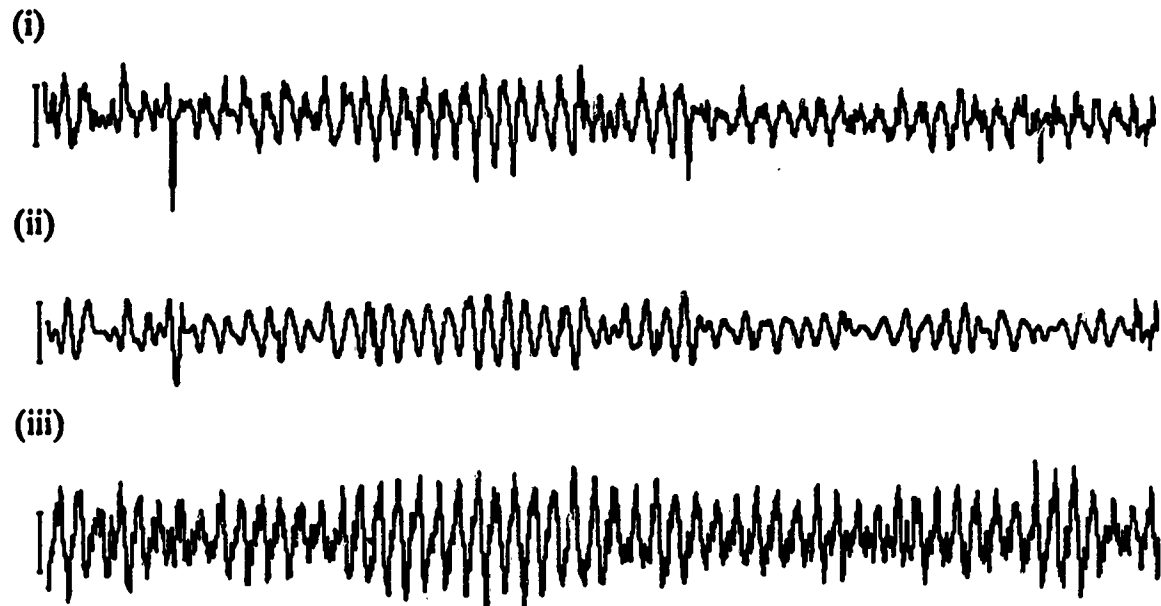
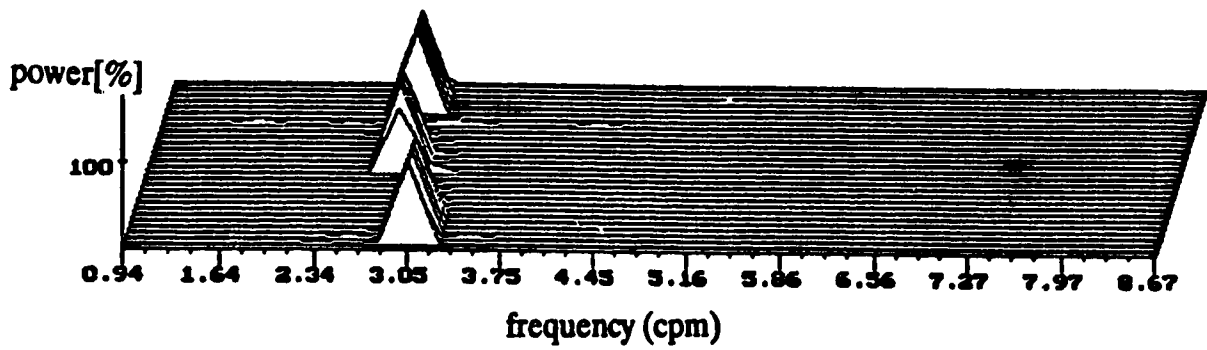


Figure 6.13c IE and EGG of Experiment B, after ingestion (80-120 mins).
(i) IE; (ii) IE after bandpass filtering; (iii) EGG channel 5.
(Volunteer C)

Volunteer C

IE: (total time: 119.47 mins; time step: 4.27 mins)



EGG

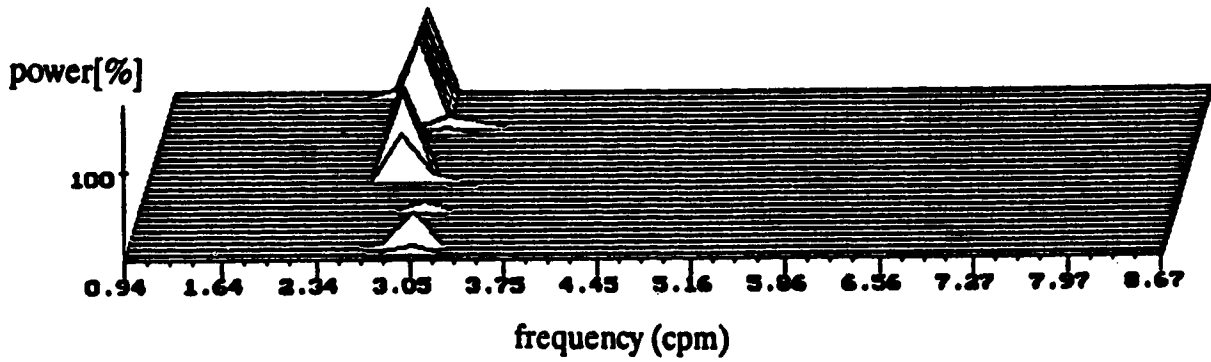


Figure 6.14 Power spectral arrays of IE and EGG after ingestion.(Volunteer C)

Volunteer C

Cross spectral arrays between IE and EGG:
(total time: 0 - 119.47 mins; time step: 4.27 mins)

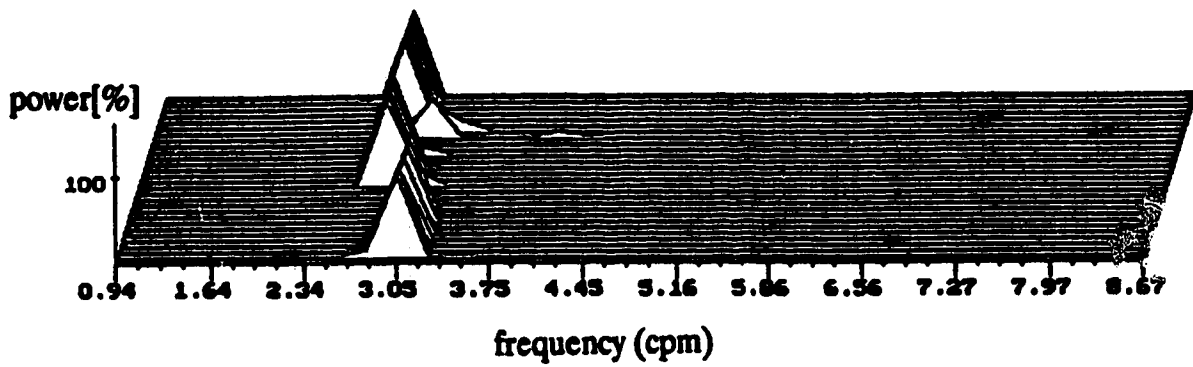


Figure 6.15 Cross spectral arrays between IE and EGG.
(after ingestion; Volunteer C)

Bibliography

- Alvarez, W.C. The electrogastrogram and what it shows. *J. Am. Med. Assoc.*, 78:1116-1119, 1922.
- Alvarez, W.C. and L.J. Machoney. Action current in the stomach and intestine. *Am. F. Physiol.*, 58:476-493, 1922.
- Avill, R., Y.F. Mangnall, N.C. Bird, B.H. Brown, D.C. Barber, A.D. Seagar, A.G. Johnson, N.W. Read. Applied Potential Tomography: A new non-invasive technique for measuring gastric emptying. *Gastroenterology*, 92:1019-1026, 1987.
- Baker, L.E. Principles of the Impedance Technique. *IEEE Engineering In Medicine and Biology Magazine*, 11-15, March 1989.
- Barber, D. C. A review of image reconstruction techniques for electrical impedance tomography. *Medical Physiology*, 16(2):162-169, 1989.
- Bhat, S. Clinical Applications, In J.G. Webster, editor, *Electrical Impedance Tomography*, chapter 13, Adam Hilger, 1990.
- Brown, B.H., R.H. Smallwood, H.L. Duthre and C.J. Stoddard. Intestinal smooth muscle electrical potentials recorded from surface electrodes. *Med. Biol Eng.*, 13:97-103, 1975.
- Challis, R.E. and R.I. Kitney. Biomedical signal processing (in four parts) Part 1 Time-domain methods. *Med. & Biol. Eng. & Comput.*, 28:509-524, 1990.
- Corazziari, E. and A. Torsoli. Radiology. In D. Kumar and S. Gustavsson, editors, *An illustrated guide to gastrointestinal motility*, chapter 4. John Wiley & Sons, 1988.
- Dawids, S. G. Evaluation of Applied Potential Tomography: A Clinician's view. *Clin. Phys. Physiol. Meas.*, 8:Suppl. A, 175-180, 1987.

- Dawids, S.G., E. U. Haxthausen, J. Hjortkjaer, J.H. Jensen, O.T. Andersen: Analysis of equipotential lines as a basis for impedance imaging. *Clin. Phys. Physiol. Meas.*, 9:Suppl. A, 21-24, 1988.
- de Vries, P.M.J.M, J.H. Meijer, K. Vlaanderen, V. Vinzer, P.L. Oe, A.J.M. Donker and H. Schneider. Measurement of Transcellular fluid shift during haemodialysis. Part 2 In vitro and clinical evaluation. *Med. & Biol. Eng & Comput.*, 27:152-158, 1989.
- Dobois, A. The Stomach. In J. Christensen, D.L. Wingate and R.A. Gregory, *A Guide to Gastrointestinal Motility*, chapter 4, J. Wright & Sons Ltd., 1983.
- Ehrlein, H. J. and L.M.A. Akkermans. Gastric Emptying. In L.M.A. Akkermans, A.G. Johnson and N.W. Read, editors, *Gastric and Gastroduodenal Motility*, chapter 6, Praeger, 1984.
- Familoni, B.O. Noninvasive Assessment of Gastric Motility. Ph.D. thesis, University of Alberta, 1986.
- Familoni, B.O., Y.J. Kingma, K.L. Bowes and K.R. Cote. Amplitude Fluctuations of Human Electrogastrogram. *IEEE Ninth Annual Conference of The Engineering in Medicine and Biology Society*, 91-93, 1987.
- Geddes, L.A., L.E. Baker and A.G. Moore. Optimal electrolytic chloriding of silver electrodes. *Med Bio Eng*, 7: 49-56, 1969.
- Geddes, L.A. Electrodes and the measurements of bioelectric events. *John Wiley and Sons Inc New York*, 1972.
- Geklof, H., Van der Shee, E.J. and Grashuis, J. L. Electrographic characteristics of interdigestive migrating complex in humans. *Am. J. Physiol.*, 250:G165-171, 1986.
- Geselowitz, David B. An Application of Electrocardiographic Lead Theory to Impedance Plethysmography. *IEEE Transactions on Bio-Medical Engineering*, 18(1):38-41, January, 1971.

- Gilbey, S. G. and P.J. Watkins. Measurement by epigastrogastric impedance of gastric emptying in diabetic autonomic neuropathy. *Diabetic Med.*, 4:122-126, 1987.
- Griffiths, H. A phantom for electrical impedance tomography. *Clin. Phys. Physiol. Meas.*, 9:Suppl. A, 15-20, 1988.
- Grundy, D. and T. Scratcherd. The role of the vagus and sympathetic nerves in the control of gastric motility. In L.M.A. Akkermans, A.G. Johnson and N.W. Read, editors, *Gastric and Gastrointestinal Motility*, chapter 2, Praeger, 1984.
- Gustavsson, Sven. Scintigraphy. In D. Kumar and S. Gustavsson, editors, *An illustrated guide to Gastrointestinal Motility*, chapter 7, 1988.
- Guyton, A. C. The Gastrointestinal Tract: Nervous Control, Movement of Food Through the Tract, and Blood Flow. In M. J. Wonsiewicz, editor, *Human Physiology and Mechanisms of Disease*, chapter 42, 1992.
- Hau, P, E.J. Woo, J.G. Webster, W.J. Tompkins. *IEEE Engineering in Medicine & Biology Society 11th Annual International Conference*, 472-273, 1989.
- Heading, R. C. Methods based on gastric intubation, X-ray and ultrasound imaging methods, indirect techniques. *Gastric and Gastrointestinal Motility*, 131-147, 1984.
- Horowitz, M. and L.M.A. Akkermans. Scintigraphic Measurement of Gastric Emptying. In N.W. Read, editor, *Gastrointestinal Motility: Which Test?*, chapter 8, Wrightson Biomedical, 1989.
- Kim, C.H. Electrogastrography. In D. Kumar and S. Gustavsson, editors, *An illustrated guide to Gastrointestinal Motility*, chapter 9, J. Wiley & Sons, 1988.
- Kim, D.W., L.E. Baker, J.A. Pearce and W.K. Kim. Origins of the Impedance Change in Impedance Cardiography by a Three-Dimensional Finite Element Model. *IEEE on Biomedical Engineering*, 35(12):993-1000, 1988.

- King, P.M. and R.C. Heading. Ultrasonography. In D. Kumar and S. Gustavsson, editors, *An illustrated guide to Gastrointestinal Motility*, chapter 8, J. Wiley and Sons, 1988.
- Kingma, Y. J., J. Lenhart, N.G. Durdle, K.L. Bowes, M.M. Chambers. Improved Ag/AgCl pressure electrodes. *Med. & Biol. Eng. & Comput.*, 21: 351-357, 1983.
- Kingma, Y. J. The Electrogastrogram and its Analysis. *CRC Critical Reviews in Biomedical Engineering*, 17(2):105-132, 1989.
- Kothapalli, B., N.G. Durdle. Multichannel Data Acquisition System for Gastric Motility. *IEEE Proceedings of the 2nd Annual IEEE Sympo. Comp. Based Med. System*, 130-133, 1989.
- Lehr, J. A Vector Derivation Useful in Impedance Plethysmographic Filtered Calculations. *IEEE Transactions on Bio-Medical Engineering*, 156-157, March, 1972.
- Lutz, H. and G. Rettenmaier. Sonographic pattern of tumors of the stomach and the intestine. *Exc. Med. Int. cong. ser.*, 277:67(abst), 1973.
- Malagelada, J.R. and V. Stanghellini. Manometric evaluation of Functional upper gut syndrome. *Gastroenterology*, 88:1223-31, 1985.
- Mamtora, H. and D.G. Thompson. Gastric Ultrasound. In N.W. Read. editor, *Gastrointestinal Motility: Which Test?*, chapter 10, Wrightson Biomedical, 1989.
- Mangnall, Y. F., A.J. Baxter, R. Avill, N.C. Bird, B.H. Brown, D.C. Barber, A.D. Seagar, A.G. Johnson and N.W. Read. Applied potential tomography: A new non-invasive technique for assessing gastric function. *Clin. Phys. Physiol. Meas.*, 8:Suppl. A, 119-129, 1987.
- Mangnall, Y. F. Clinical Uses of Applied Potential Tomography and Impedance Epigastrography as Methods of Measuring Gastric Emptying. In N.W. Read, editor, *Gastrointestinal Motility: Which Test?*, chapter 9, Wrightson Biomedical, 1989.

- McClelland, G. R. and J.A. Sutton. Epigastric Impedance: a non invasive method for the assessment of gastric emptying and motility. *Gut*, 26:607-614, 1985.
- McClelland, G.R. and J.A. Sutton. A comparison of the gastric and central nervous system effects of two substituted benzamide in normal volunteers. *Br. J. Clin. Pharm.*, 21:503-509, 1986.
- Nagel, L.W. SPICE2: A computer Program to Simulate Semiconductor Circuits., *Memorandum No. ERL-M520, 9, Electronic Research Lab, College of Engineering, University of California, Berkeley, CA, May, 1975.*
- Newell, J.C., D. Isaacson and D.G. Gisser. Rapid Assessment of Electrode Characteristics for Impedance Imaging. *IEEE Transactions on Biomedical Engineering*, 37(7):735-737, July, 1990.
- Nyboer, J., Q. Bango, A. Barnett and R.H. Halsey. Radiocardiograms. the Electrical Impedance changes of the Heart in Relation to Electrocardiograms and Heart sounds. *American Society of Clinical Investigation*. Vol 19, 113, 1940.
- Patterson, R. P. Source of the Thoracic Cardiogenic Electrical Impedance Signal as determined by a model. *Medical & Biological Engineering & Computing*, 411-417, September, 1985.
- Patterson, R.P., L. Wang, B. Raza and K. Wood. Mapping the cardiogenic impedance signal on the thoracic surface. *Med. & Bio. Eng. & Comput.*, 28:212-216, 1990.
- Penney, B.C. Theory and Cardiac Applications of Electrical Impedance Measurements. *CRC Critical Reviews in Biomedical Engineering*. 13(3):227-272, 1986.
- Qiao, Z.G. and L. Mørkrid. Continuous estimation of parameters in skin electrical admittance from simultaneous measurements at two different frequencies. *Med. & Biol. Eng. & Comput.*, 26:633-640, 1988.
- Read, N.W. The Design of a Gastrointestinal Motility Lab. In N.W. Read, editor, *Gastrointestinal Motility: Which test?*, chapter 1, Wrightson Biomedical, 1989.

- Rosell, J., J. Colominas, P. Riu, R. Pallas-Areny and J.G. Webster. Skin Impedance From 1Hz to 1MHz. *IEEE Transactions on Biomedical Engineering*, 35(8):649-651, August, 1988.
- Sahalos, J.N., A. Nicolaidis and N. Gotsis N. The electrical impedance of the human thorax as a guide in evaluation of intrathoracic fluid volume. *Phys. Med. Biol.*, 31:425-439, 1986.
- Sarna, S.K. In vivo myoelectric activity: methods, analysis and interpretation. *The Gastrointestinal System*, 2:817, 1989.
- Schulze-Delrieu, K., H.J. Ehrlein, A.L. Blum. Mechanics of the Pylorus. In L.M.A. Akkermans, A.G. Johnson and N.W. Read, editors, *Gastric and Gastroduodenal Motility*, chapter 7, Praeger, 1984.
- Sheiner, H.L. Gastric Motility. *Scientific Basis of Gastroenterology*, 440-459, 1979.
- Smout, A.J.P.M. and E.J. Van der Schee. Electrogastrography. In N.W. Read, editor, *Gastrointestinal Motility: Which Test?*, chapter 12, Wrightson Biomedical, 1989.
- Smout, A.J.P.M., E.J. Van der Schee and J.L. Grashuis. What is measured in Electrogastrography? *Dig. Dis. Sci.*, 25:179-187, 1980.
- Soper, N.F. and M.G. Sarr. Electromyography. In D.Kumar and S. Gustavsson, editors, *An illustrated guide to Gastrointestinal Motility*, chapter 9, J. Wiley & Sons, 1988.
- Stoddard, C. J. Intraluminal Myoelectrical recordings. In L.M.A. Akkermans, A.G. Johnson and N.W. Read, editors, *Gastric and Gastroduodenal Motility*, chapter 12, Praeger, 1984.
- Sutton, J.A. Impedance. In D. Kumar and S.Gustavsson, editors, *An illustrated guide to Gastrointestinal Motility*, chapter 10, J. Wiley & Sons, 1988.
- Vlachogiannis, M., G. Kyriakon, C. Coucourlis, N. Gotsis and J.N. Sahalos. Determination of the physical state of the human thorax by means of impedance plethysmography. *Archiv für Elektrotechnik*, 71:99-105, 1988.

Weisbrodt, N.W. Basic Control Mechanisms. In L.M.A. Akkermans, A.G. Johnson and N.W. Read, editors, *Gastric and Gastroduodenal Motility*, chapter 1, Praeger, 1984.